Journal of Autoimmunity 119 (2021) 102610

Contents lists available at ScienceDirect

Journal of Autoimmunity

journal homepage: www.elsevier.com/locate/jautimm

Histone deacetylase 1 controls CD4$^+$ T cell trafficking in autoinflammatory diseases

Patricia Hamminger [a], Luca Marchetti [b], Teresa Preglej [a,l], René Platzer [c], Ci Zhu [a,d], Anton Kamnev [e,f], Ramona Rica [a], Valentina Stolz [a], Lisa Sandner [a], Marlis Alteneder [a], Elisa Kaba [b], Darina Waltenberger [a], Johannes B. Huppa [c], Michael Trauner [d], Christoph Bock [g,h], Ruth Lyck [b], Jan Bauer [i], Loïc Dupré [e,f,j], Christian Seiser [k], Nicole Boucheron [a], Britta Engelhardt [b], Wilfried Ellmeier [a,*]

[a] Division of Immunobiology, Institute of Immunology, Center for Pathophysiology, Infectiology and Immunology, Medical University of Vienna, Vienna, Austria
[b] Theodor Kocher Institute, University of Bern, Bern, Switzerland
[c] Institute of Hygiene and Applied Immunology, Center for Pathophysiology, Infectiology and Immunology, Medical University of Vienna, Vienna, Austria
[d] Hans Popper Laboratory of Molecular Hepatology, Division of Gastroenterology and Hepatology, Department of Internal Medicine III, Medical University of Vienna, Vienna, Austria
[e] Ludwig Boltzmann Institute for Rare and Undiagnosed Diseases, Vienna, Austria
[f] Department of Dermatology, Medical University of Vienna, Vienna, Austria
[g] CeMM Research Center for Molecular Medicine of the Austrian Academy of Sciences, Vienna, Austria
[h] Institute of Artificial Intelligence and Decision Support, Center for Medical Statistics, Informatics, and Intelligent Systems, Medical University of Vienna, Vienna, Austria
[i] Department of Neuroimmunology, Center for Brain Research, Medical University of Vienna, Austria
[j] Toulouse Institute for Infectious and Inflammatory Diseases (INFINITy), INSERM UMR1291, CNRS UMR5051, Toulouse III Paul Sabatier University, Toulouse, France
[k] Division of Cell and Developmental Biology, Center for Anatomy and Cell Biology, Medical University of Vienna, Vienna, Austria
[l] Current Address: Division of Rheumatology, Medical University of Vienna, Vienna, Austria

ARTICLE INFO

Keywords:
Histone deacetylases
Experimental autoimmune encephalomyelitis
Adoptive CD4$^+$ T cell transfer colitis
T cell migration

ABSTRACT

CD4$^+$ T cell trafficking is a fundamental property of adaptive immunity. In this study, we uncover a novel role for histone deacetylase 1 (HDAC1) in controlling effector CD4$^+$ T cell migration, thereby providing mechanistic insight into why a T cell-specific deletion of HDAC1 protects against experimental autoimmune encephalomyelitis (EAE). HDAC1-deficient CD4$^+$ T cells downregulated genes associated with leukocyte extravasation. *In vitro*, HDAC1-deficient CD4$^+$ T cells displayed aberrant morphology and migration on surfaces coated with integrin LFA-1 ligand ICAM-1 and showed an impaired ability to arrest on and to migrate across a monolayer of primary mouse brain microvascular endothelial cells under physiological flow. Moreover, HDAC1 deficiency reduced homing of CD4$^+$ T cells into the intestinal epithelium and lamina propria preventing weight-loss, crypt damage and intestinal inflammation in adoptive CD4$^+$ T cell transfer colitis. This correlated with reduced expression levels of LFA-1 integrin chains CD11a and CD18 as well as of selectin ligands CD43, CD44 and CD162 on transferred circulating HDAC1-deficient CD4$^+$ T cells. Our data reveal that HDAC1 controls T cell-mediated autoimmunity via the regulation of CD4$^+$ T cell trafficking into the CNS and intestinal tissues.

* Corresponding author. Division of Immunobiology, Institute of Immunology, Center for Pathophysiology, Infectiology and Immunology, Medical University of Vienna, Lazarettgasse 19, 1090, Vienna, Austria.

E-mail addresses: patricia.hamminger@meduniwien.ac.at (P. Hamminger), lmarchetti90@gmail.com (L. Marchetti), teresa.preglej@meduniwien.ac.at (T. Preglej), rene.platzer@meduniwien.ac.at (R. Platzer), ci.zhu@meduniwien.ac.at (C. Zhu), anton.kamnev@rud.lbg.ac.at (A. Kamnev), ramona.rica@meduniwien.ac.at (R. Rica), valentina.stolz@meduniwien.ac.at (V. Stolz), lisa.sandner@meduniwien.ac.at (L. Sandner), marlis.alteneder@meduniwien.ac.at (M. Alteneder), elisa.kaba@tki.unibe.ch (E. Kaba), darina.waltenberger@meduniwien.ac.at (D. Waltenberger), johannes.huppa@meduniwien.ac.at (J.B. Huppa), michael.trauner@meduniwien.ac.at (M. Trauner), cbock@cemm.oeaw.ac.at (C. Bock), ruth.lyck@tki.unibe.ch (R. Lyck), jan.bauer@meduniwien.ac.at (J. Bauer), loic.dupre@rud.lbg.ac.at (L. Dupré), christian.seiser@univie.ac.at (C. Seiser), nicole.boucheron@meduniwien.ac.at (N. Boucheron), britta.engelhardt@tki.unibe.ch (B. Engelhardt), wilfried.ellmeier@meduniwien.ac.at, wilfried.ellmeier@meduniwien.ac.at (W. Ellmeier).

https://doi.org/10.1016/j.jaut.2021.102610
Received 13 December 2020; Received in revised form 26 January 2021; Accepted 27 January 2021
Available online 20 February 2021

1. Introduction

T cell trafficking is a fundamental property of adaptive immunity. The migration of effector $CD4^+$ T cells towards inflamed sites and tissues is key for the coordination of a proper host defense against pathogens. However, the extravasation of dysregulated or autoreactive T cells into tissues can lead to immune-mediated diseases including autoimmunity. A well-explored murine model for studying $CD4^+$ T cell migration in the context of autoimmunity is experimental autoimmune encephalomyelitis (EAE), a Th1/Th17 cell-driven autoinflammatory process that leads to inflammation and demyelination in the CNS [1,2]. EAE is often used as a disease model for human multiple sclerosis (MS), even though it deviates to some extent with regard to the complex disease pathology of MS [3]. In EAE, activated $CD4^+$ T cells migrate from lymph nodes via the blood and subsequently infiltrate the CNS via several routes that include crossing the endothelial blood-brain barrier (BBB), the epithelial blood-cerebrospinal fluid barrier of the choroid plexus and the subarachnoid space [2,4]. T cell migration at the BBB (or at other endothelial barriers) is a multistep process that relies on sequential steps of lymphocyte rolling, arrest, crawling and diapedesis across the endothelial layer [5]. These steps are regulated via the interaction of cell adhesion molecules and their ligands expressed on activated $CD4^+$ T cells and the inflamed endothelium. Binding of glycosylated selectin ligands, such as PSGL-1, CD43 and CD44, expressed on activated $CD4^+$ T cells, to endothelial P- and E-selectin is essential for capture/rolling [6,7]. Further, following the activation of integrins, the interaction of the $\alpha_L\beta_2$-integrin lymphocyte function-associated antigen-1 (LFA-1, formed by the CD11a and CD18 chains) with intercellular adhesion molecule-1 (ICAM-1) as well as ICAM-2 expressed on endothelial cells and of the $\alpha_4\beta_1$-integrin very late antigen-4 (VLA-4) with endothelial vascular cell adhesion molecule-1 (VCAM-1), respectively, mediates T cell arrest. Moreover, LFA-1 binding to ICAM-1 and ICAM-2 mediates T cell crawling on the BBB [8–16]. The importance of integrins in this process has been exploited for therapeutic purposes, with the integrin α4 chain blocking monoclonal antibody natalizumab approved for MS therapy [17,18].

The differentiation of naïve $CD4^+$ T cells into effector Th subsets is accompanied by the induction and maintenance of lineage-specific gene expression programs. During these differentiation processes, there also is an induction of genes essential for migration and homing of effector $CD4^+$ T cells into inflamed tissues. These Th subset-specific transcriptional programs are in part controlled by epigenetic processes that include the reversible acetylation of histones mediated by the opposing activities of histone acetyltransferases (HATs) and histone deacetylases (HDACs). In addition to chromatin-mediated effects via modifying histones and thus regulating DNA accessibility, reversible acetylation also targets a large number of non-histone proteins which in turn is affecting their functionality [19,20]. The HDAC family consists of 18 members that are grouped into 4 classes and several HDACs have important functions in $CD4^+$ T cells [19]. We have recently shown that the class I member HDAC1 in T cells is key for the induction of autoinflammatory diseases. Conditional deletion of HDAC1 in T cells (using the *Cd4*-Cre deleter strain; *Hdac1*$^{fl/fl}$ x *Cd4*-Cre, designated as HDAC1^{cKO}) conveys resistance to the induction of EAE, even in the absence of $CD25^+$ regulatory T (T_{reg}) cells. Mixed WT and HDAC1^{cKO} bone marrow chimeric mice are susceptible for EAE induction, however predominantly WT and only a small fraction of HDAC1^{cKO} $CD4^+$ T cells infiltrated the CNS [21]. These data indicate effector $CD4^+$ T cell-intrinsic defects. Moreover, naïve HDAC1-deficient $CD4^+$ T cells differentiate into Th17 cells *in vitro* and display normal IL-17A and RORγt expression [21] and HDAC1^{cKO} Th1 cells even produce elevated levels of IFNγ compared to WT Th1 cells [22,23]. Although *in vivo* Th differentiation was not directly investigated, these results suggest that HDAC1 deficiency did not block Th1/Th17 differentiation in EAE-inducing conditions. Similar to the protective effect observed for EAE, HDAC1^{cKO} mice are also protected from the induction of collagen-induced arthritis (CIA) [24]. Together, these previous studies demonstrate that HDAC1 is a key regulator of T cell-mediated autoimmunity and inflammation. However, the underlying mechanisms have not been revealed.

In this study, we employed EAE as well as adoptive transfer colitis as model systems to investigate how HDAC1 controls $CD4^+$ T cell function and why loss of HDAC1 protects against autoinflammatory diseases. Using the myelin oligodendrocyte glycoprotein 2D2 TCR transgenic system we showed that the *in vivo* activation and expansion of HDAC1-deficient $CD4^+$ T cells was normal at the induction phase of EAE. However, *in vivo*-activated 2D2-HDAC1^{cKO} T cells downregulated genes that mediate leukocyte extravasation including genes that encode for integrin LFA-1, key selectin ligands as well as cytoskeletal proteins. HDAC1^{cKO} $CD4^+$ T cells displayed aberrant migratory features due to deficient arrest on endothelial barriers and a subsequent reduction in transendothelial migration, findings that were in line with downregulated leukocyte extravasation pathways. Hence, LFA-1-dependent cellular responses are impaired in the absence of HDAC1, which restricts $CD4^+$ T cells from extravasation at endothelial barriers into the CNS. Moreover, adoptively transferred HDAC1-deficient $CD4^+$ T cells failed to migrate into the intestinal epithelium and lamina propria in an adoptive $CD4^+$ T cell transfer colitis model resulting in abolished weight-loss, intestinal inflammation and crypt damage in recipient mice. The lack of disease correlated with reduced expression levels of LFA-1 integrin chains CD11a and CD18 as well as of selectin ligands CD43, CD44 and CD162 on transferred circulating HDAC1-deficient $CD4^+$ T cells. This indicates that HDAC1 is a key regulatory factor that also controls integrin as well as selectin ligand expression in the context of intestinal inflammation. Taken together, our findings identify a critical function for HDAC1 in regulating $CD4^+$ T cell trafficking.

2. Materials and methods

2.1. Mice

Hdac1$^{fl/fl}$*Cd4*-Cre (HDAC1^{cKO}) mice were previously described [22] (Mouse Genome Informatics MGI: 4440556) and floxed *Hdac1* mice were kindly provided by Patrick Matthias. *Cd4*-Cre mice (MGI:2386448) were kindly provided by Chris Wilson. 2D2 TCR MOG transgenic mice (2D2) recognizing MOG_{35-55} [25] (MGI:3700794) were kindly provided by Gernot Schabbauer. 2D2 mice were crossed to *Hdac1*$^{fl/fl}$*Cd4*-Cre mice to generate 2D2 x *Hdac1*$^{fl/fl}$*Cd4*-Cre (2D2- HDAC1^{cKO}) mice. CD45.1 and *Rag2*$^{-/-}$ mice were kindly provided by Jochen Hühn. Mice were analyzed between 8 and 12 weeks of age. Experiments were performed with mice of mixed sex unless otherwise stated. Animal experiments were evaluated by the ethics committee of the Medical University of Vienna and approved by the Austrian authorities (GZ: BMWF-66.009/0103-WF/II/3b/2014, GZ:BMWF-66.009/0105-WF/II/3b/2014, GZ:BMBFW-66.009/0039-WF/II/3b/2019, GZ:BMBFW-66.009/0041-WF/II/3b/2019). Mice were bred and maintained in the preclinical research facility of the Medical University of Vienna. Animal husbandry and experimentation were performed in compliance with national laws and according to FELASA and ARRIVE guidelines.

2.2. Induction of experimental autoimmune encephalomyelitis

Female 2D2-WT and 2D2-HDAC1^{cKO} mice were subcutaneously (s.c.) injected with 100 μl of an emulsion of 500 μg/ml MOG_{35-55} peptide (M4939, Sigma Aldrich) in Aq. dest. and complete Freund's adjuvant (incomplete Freund's adjuvant (Sigma) supplemented with 5 mg/ml heat-killed *Mycobacterium tuberculosis* (strain H37Ra; Difco)) into the left and right flank. On the day of immunization as well as 2 days later mice were injected intraperitoneally (i.p.) with 400 ng pertussis toxin (Sigma Aldrich). Disease progression was monitored daily and assessed according to the following disease scores: 0 = unaffected; 0.5 = incomplete limp tail; 1 = complete limp tail; 1.5 = limp tail and hind limb weakness (mild wobbly walk); 2 = limp tail and weakness of hind legs (wobbly

walk) 2.5 = limp tail and dragging of hind legs; 3 = no movement or complete dragging of one leg; 3.5 = complete bilateral paralysis of hind legs; 4 = limp tail and complete paralysis of hind legs, or mouse is unable to turn upright when placed on its side, or mouse is dragging the complete hindquarter; 4.5 = limp tail, complete hind leg and partial front leg paralysis but mouse is alert and feeding; 5 = complete hind and partial front leg paralysis, no movement.

2.3. Neuropathological evaluation

Immunohistochemistry was performed with a biotin-avidin system using biotinylated anti-rabbit immunoglobulins (Amersham, Birmingham UK) as secondary antibodies followed by avidin-HRP (Cat. No. A3151, Sigma, St. Louis Mo). T cells were stained with anti-CD3 antibodies (Cat. No. A452, Dakopatts, Denmark). Quantifications were performed by using a morphometric grid. To determine the extent of inflammation, the number of $CD3^+$ T cells was quantified in three lumbar spinal cross sections and divided by the volume (mm^2) of these three sections. The extent of demyelination was evaluated on tissue sections stained with Luxol Fast Blue (LFB) combined with Periodic Acid Schiff (PAS) for myelin and myelin degradation products. Areas of demyelination were determined on stained spinal cord cross sections (on average 10–15 sections) and were expressed as % of total spinal cord white matter area.

2.4. Flow cytometry antibodies

The following anti-mouse antibodies were used for flow cytometry: B220 (clone: RA3-6B2), CD11a (clone: M17/4), CD69 (clone: H1·2F3), GM-CSF (clone: MP1-22E9), TCRβ (clone: H57-597), all from Thermo Fisher Scientific; CD18 (clone: M18/2), CD4 (clone: RM4-5), CD44 (clone: IM7), CD45.1 (clone: A20), CD45.2 (clone: 104), CD62L (clone: MEL-14), CD90.2 (clone: 53–2.), IFNγ (clone: XMG1.2), IL-17 (clone: TC11-18H10.1), IL-2 (clone: JES6-5H4), Vα3.2 (clone: RR3-16), Vβ11 (clone: KT11), all from Biolegend; CD162 (clone: 2PH1), CD43 (clone: S7), CD25 (clone: PC61), all from BD Biosciences.

2.5. Purification of naïve $CD4^+$ T cells

Single cell suspensions of spleens, axillary, brachial and inguinal lymph nodes were obtained by mashing the organs though a 70 μm cell strainer (Corning) in PBS supplemented with 2% fetal bovine serum (FBS) (Biowest) (PBS/FBS). Red blood cell lysis was performed using BD Pharm Lyse™ (BD Biosciences) according to the manufacturer's instructions. $CD4^+$ T cells were enriched by incubation of the cell suspension with a cocktail containing biotinylated antibodies (Gr-1, B220, NK1.1, CD11b, CD11c, CD8a, and TER-119) following negative depletion using streptavidin negative selection beads (MagniSort SAV Negative Selection beads; Invitrogen). Cells were sorted for naïve $CD4^+$ T cells ($CD25^-CD44^{lo}CD62L^+$) using a BD FACSAriaII (BD Biosciences) or a SH800 (SONY). For some experiments naïve $CD4^+$ T cells were isolated using the EasySep™ Mouse Naïve $CD4^+$ T Cell Isolation Kit according to the manufacturer's instructions. Biotinylated antibodies against Ly-6G/Ly-6C (clone: RB6-8C5), CD45R/B220 (clone: RA3-6B2), NK1.1 (clone: PK136), CD11c (clone: N418), CD11b (clone: MEL1/70), CD8α (clone: 53–6.7) and TER-119 (clone: TER-119) were purchased from Biolegend.

2.6. Extracellular and intracellular staining

For intracellular cytokine detection, *ex vivo* isolated or *in vitro* cultured cells (1×10^6 cells/ml) were stimulated for 4 h with PMA (25 ng/ml) and ionomycin (750 ng/ml) (both from Sigma-Aldrich) in the presence of GolgiStop (BD Biosciences). Cells were incubated with Fc Block (1:250 in PBS, BD Biosciences) prior to extracellular staining. Dead cells were excluded by Fixable Viability Dye eFluor™ 506 (Thermo Fisher Scientific) or Zombie NIR™ Fixable Viability Dye (423105, Biolegend) staining. Cells were stained with extracellular antibodies on ice in the dark for 30 min. For subsequent intracellular cytokine staining cells were fixed with Cytofix™ Fixation Buffer (BD Biosciences), permeabilized with Perm/Wash Buffer (BD Biosciences) and analyzed with a BD LSRFortessa or BD LSRII cytometer and FlowJo 10.2 software.

2.7. In vivo $CD4^+$ T cell activation and expansion assays

6×10^5 naïve 2D2-WT or 2D2-$HDAC1^{cKO}$ $CD4^+$ T cells ($CD45.1^-CD45.2^+$) were injected intravenously (i.v.) into $CD45.1^+CD45.2^+$ recipient mice. 18 h after cell transfer mice were immunized via injecting 50 μl of a 1:1 emulsion of 1 mg/ml MOG_{35-55} peptide (M4939, Sigma Aldrich) in Aq. dest.) and complete Freund's adjuvant (incomplete Freund's adjuvant (Sigma) supplemented with 10 mg/ml heat-killed *Mycobacterium tuberculosis* (strain H37Ra; Difco)) into the right hind paw. Spleen, draining (popliteal) and pooled peripheral lymph nodes were harvested 2 or 4 days later and single cell suspensions prepared. Cells were stained for extracellular activation markers and analyzed with BD LSRFortessa (BD Biosciences) and FlowJo 10.2 software.

2.8. Transwell migration assays

Naïve $CD4^+$ T cells were differentiated into Th17 cells with plate-bound anti-CD3Ɛ (1 μg/ml; BD Biosciences) and anti-CD28 (3 μg/ml; BD Biosciences) on 48-well-plates (0.3×10^6 cells/well) in 1 ml T cell medium/well (RPMI-1640, 10% FBS (Biowest), antibiotics, 50 mM β-mercaptoethanol) supplemented with 2 ng/ml TGFβ (Biolegend) and 10 μg/ml IL-6 (Peprotech). On day 2 of culture cells were differentially labelled with cell proliferation dye eFluor™ 670 and eFluor™ 450 (65-0840-85 and 65-0842-85, eBioscience) and cultured for one additional day. Within each experiment labels were swapped between WT and $HDAC1^{cKO}$ to control for dye effects. Cells were washed with PBS, quantified and mixed at a 1:1 ratio. The cells were resuspended (3×10^6 cells/ml) in RPMI supplemented with 1% fatty acid-free BSA and 10 mM HEPES. 100 μl of this cell suspension was added to the top chambers of 24-well transwell plates with 3 μm pores (Corning). The cells were allowed to migrate for 4 h at 37 °C in the presence of 1 μg/ml CCL21 or 1 μg/ml CCL20 (both from Peprotech) in RPMI with 1% fatty acid-free BSA and 10 mM HEPES in the lower well. Subsequently, migrated cells were collected from the bottom well and the ratio of WT and $HDAC1^{cKO}$ cells was quantified for a fixed period of time (2 min) with a BD LSRFortessa (BD Biosciences) and the resulting ratios normalized for the input ratio.

2.9. Endothelioma cell line bEnd.5

The bEnd.5 mouse brain endothelioma cell line was described previously [16]. Prior to culturing T25 flasks were coated with 0.1% Gelatine for 30 min at 37 °C and then washed with PBS. 2×10^6 cells were then grown in Dulbecco's modified Eagle's medium (DMEM 4500 mg/L Glucose w/o Na-Pyruvate) supplemented with 10% FCS, 50 μM β-mercaptoethanol, 4 mM L-glutamine, 1 mM sodium pyruvate, antibiotics and 1 x nonessential amino acids at 37 °C and 10% CO_2. bEnd.5 cells were passaged only following confluency at a maximal splitting ratio of 1:4. For static transendothelial migration assays 24-well transwell inserts with 5 μm pores were coated with 50 μl laminin (50 μg/ml in PBS) at 20 °C for 30 min and then air-dried for 60 min under sterile conditions. bEnd.5 cells were harvested by washing the cells with 1x HBSS supplemented with 25 mM HEPES and 5 mM EDTA, trypsinized and washed in wash buffer (DMEM supplemented with 25 mM HEPES and 5% FCS). 5×10^4 cells were plated on the transwell inserts and cultured for one more day until stimulation.

2.10. Primary mouse brain microvascular endothelial cells

Primary Mouse Brain Microvascular Endothelial Cells (pMBMECs) were isolated from 4 to 8 weeks old C57BL/6J mice and cultured as described [16,26]. Capillaries from one brain were used for seeding 3 matrigel-coated Ibidi μ-dishes with cloning rings for *in vitro* live cell imaging under flow conditions or two 24-well filter inserts for static transendothelial migration assays. pMBMECs were cultured for 6 days at 37 °C and 10% CO_2 until stimulation.

2.11. $CD4^+$ T cell transendothelial migration assays

bEnd.5 cells were stimulated with 10 μg/ml LPS (*Escherichia coli* O55:B5; Sigma) and pMBMECs with 10 ng/ml TNF-α (Peprotech) 18 h before starting the assays followed by a washing step with migration assay medium (DMEM supplemented with 2% L-glutamine, 25 mM HEPES and 5% FCS). Dye-labelled WT and $HDAC1^{cKO}$ Th17 cells were prepared as described above and mixed at a 1:1 ratio. Labels were swapped between WT and $HDAC1^{cKO}$ within each experiment to control for dye effects. The cells were resuspended (3×10^6 cells/ml) in migration assay medium and 100 μl of the Th17 cell suspension were added to the top chambers of 24-well transwell plates. The cells were allowed to migrate across endothelial monolayers for 4 h at 37 °C towards the lower well. Transmigrated cells were collected from the lower well and quantified and normalized as described above.

2.12. $CD4^+$ T cell in vitro microscopy assay

For analysis of cell morphology, WT and $HDAC1^{cKO}$ Th17 cells were plated on 384 well-plates (PerkinElmer) pre-coated with 6 μg/ml recombinant ICAM-1. Immediately after plating the cells were gently pushed towards the coated surface by short centrifugation (70 g, 20 s) and let to adhere and migrate for 30 min at 37 °C. Following incubation, cells were fixed with 4% Formalin (Pierce) in growth media for 15 min at 37 °C and incubated 15 min at 37 °C in permeabilization buffer (eBioscience) supplemented with 2% heat inactivated FBS (HyClone). Next, cells were stained at 4 °C with Phalloidin-AF488 (1:500; Cell Signaling Technology) and DAPI (5 μg/ml, Thermo Fisher Scientific). Finally, cells were washed with PBS and stored in PBS at 4 °C. Stained cells were imaged using a PerkinElmer Opera Phenix high-content screening system equipped with a 40x lense (1.1NA, water immersion), confocal unit (Yokogawa CSU-X) and solid-state laser illumination (405 nm, 488 nm). In order to assess the cell morphology 9 images per well were recorded (1080 × 1080 pxl; 320 nm/pxl resolution; 3x Z stacks with dZ = 0.5 μm near the coverslip surface). Cell area and total amount of F-actin per cell were quantified using custom written pipelines in Fiji and CellProfiler. Resulting measurements were then further processed using custom written Python scripts.

2.13. In vitro live cell imaging under flow conditions

In vitro live cell imaging was performed as described before [27]. pMBMEC monolayers were stimulated with 10 ng/ml TNF-α or 20 ng/ml IL1-β 18 h before starting the assays. WT and $HDAC1^{cKO}$ Th17 cells were generated as described above and resuspended in RPMI-1640 supplemented with 10% FBS (Thermo Fisher Scientific), 10 U/ml penicillin-streptomycin, 2 mM L-glutamine, 1% (v/v) non-essential amino acids, 1 mM sodium pyruvate and 50 μM β-mercaptoethanol at a concentration of 1×10^6 cells/ml. The concentration was confirmed once more before and after each experiment by quantifying live cells in a counting chamber using trypan blue. Th17 cells were flushed on top of the monolayer and accumulation on pMBMECs within the flow chamber was enabled by adjusting the flow to low shear (0.1 dyn/cm^2) for the first 5 min followed by physiological shear flow (1.5 dyn/cm^2) for 25 more minutes. An inverted microscope (AxioObserver, Zeiss, Feldbach, Switzerland) with a 10x magnification objective was used for phase contrast image acquisition every 10 s using a monochrome charge-coupled device camera (AxioCam MRm Rev, Carl Zeiss). The temperature was maintained at 37 °C throughout the experiment. Image analysis was blinded and performed using ImageJ software (National Institute of Health, Bethesda, MD, USA). Arrested cells per field of view (FOV) were quantified 20 s after applying physiological flow and were further categorized into T cells detaching, probing (cells remaining situated at the same position and probing their surrounding via protrusions), crawling or undergoing diapedesis (cells migrating across the pMBMEC monolayer) within the recording period. T cells that crawled out of the FOV were not categorized.

2.14. Migration assay on ICAM-1

Glass slides (24 mm × 50 mm #1.5 borosilicate, VWR) were attached to the bottom of 8-well LabTek chambers (Nunc). The chambers were coated with 6 μg/ml recombinant murine ICAM-1 and 2 μg/ml CXCL-12 (Peprotech) in coating buffer (20 mM Tris pH 9.0, 159 mM NaCl, 2 mM MgCl2) for 16 h at 4 °C or 4 h at room temperature and then gently rinsed with coating buffer. Subsequently the chambers were filled with prewarmed (37 °C) imaging buffer (HBSS, Thermo Fisher Scientific, supplemented with 2 mM $CaCl_2$, 2 mM $MgCl_2$ and 2% FCS). Migration assays of Th17 cells on ICAM-1- and CXCL-12-coated surfaces were performed with some adaptions as described [28]. WT or $HDAC1^{cKO}$ Th17 cells were labelled with either 100 nM Carboxyfluorescein succinimidyl ester (CFSE, Thermo Fisher Scientific) or 500 nM proliferation dye eFluor™ 670 (eF670, eBioscience) for 10 min at 37 °C and subsequently washed with imaging buffer. To compensate for dye-related effects, fluorescence dyes were swapped and the tracking data pooled within one experiment. 0.5×10^6 fluorescently-labelled WT and $HDAC1^{cKO}$ Th17 cells were premixed in a 1:1 ratio and allowed to adhere to the glass slides for 10 min. Migration of WT and $HDAC1^{cKO}$ Th17 cells was recorded simultaneously for 30 min with an image every 10 s. CFSE and eF670 were excited with a monochromatic light source (Leica EL6000) coupled to an inverted microscope (Leica DMI 5000) operated with a 20x objective (Leica) and excitation filters 474/27 (Chroma) and 635/18 (Chroma). A temperature control system (Leica) was used to adjust the temperature to 37 °C. Microscopy images were processed and analyzed with the open-source image processing package Fiji [29] and Matlab (MathWorks). Cells were localized and tracked using a custom written code in Matlab [30]. Cell trajectories which were visible for more than 10 frames (out of 181 frames) were included in the analysis.

2.15. Low-input RNA sequencing of in vivo activated $CD4^+2D2^+$ T cells

6×10^5 naïve 2D2-WT or 2D2-$HDAC1^{cKO}$ $CD4^+$ T cells ($CD45.2^+$) were transferred (i.v.) into $CD45.1^+$ recipient mice. 18 h after cell transfer mice were immunized into the right hind paw with 50 μl of a 1:1 emulsion of 1 mg/ml MOG_{35-55} peptide (M4939, Sigma Aldrich) in Aq. dest.) and complete Freund's adjuvant (incomplete Freund's adjuvant (Sigma) supplemented with 10 mg/ml heat-killed *Mycobacterium tuberculosis* (strain H37Ra; Difco)). Draining (popliteal) lymph nodes were isolated 4 days later and single cell suspensions prepared. Two mice were pooled for one biological replicate and three biological replicates were generated for each genotype. 500 $CD45.2^+$ $2D2^+$ $CD4^+$ T cells were sorted into 96 wells filled with 3.8 μl 0.2% (vol/vol) Triton X-100 solution and 0.2 μl RNase inhibitor (2313A, Clontech). RNA isolation, library preparation and sequencing was performed by the Biomedical Sequencing facility at CeMM with the Smart-seq2 assay [31]. The libraries were sequenced using the Illumina HiSeq 3000 platform and the 50-bp single-read configuration.

2.16. Bioinformatic analysis

Raw sequencing data were processed with Illumina2 bam-tools 1.17

to generate sample-specific, unaligned BAM files. Sequence reads were mapped onto the mouse genome assembly build mm10 (GRCm38) using TopHat 2.0.13 [32]. Gene expression values (reads per kilobase exon per million mapped reads) were calculated with Cufflinks 2.2.1 [33]. Data analysis was performed using Ingenuity Pathway Analysis (Qiagen IPA) revealing significantly dysregulated pathways ($-2 \geq$ Z score ≥ 2; $P \leq 0.05$).

2.17. Adoptive $CD4^+$ T cell transfer colitis

0.5×10^6 naïve WT or $HDAC1^{cKO}$ $CD4^+$ T cells were intravenously (i.v.) injected into *Rag2*$^{-/-}$ recipient mice. Weight loss was assessed weekly and recipients were analyzed 6 weeks after cell transfer. Spleen, mesenteric lymph nodes, small intestinal lamina propria (SI-LP) cells and small intestinal intraepithelial lymphocytes (SI-IEL) cells were isolated and analyzed as described before [34]. Histological analysis was performed on isolated colon tissue using "swiss rolls" as described previously [71][].

2.18. Colon histology and multicolor immunofluorescence microscopy

Following fixation in 7.5% formaldehyde tissue samples of 5 μm thickness were stained with hematoxylin and eosin. For immunofluorescence staining, tissue sections were heated to 95 °C in antigen retrieval buffer (citrate buffer, pH 6) and blocked in 10% goat serum in PBS. Sections were then stained with primary rabbit anti-CD3 (Novus) and anti-E-cadherin (eBioscience) followed by secondary Alexa Fluor 488 anti-rabbit and Alexa Fluor 647 anti-mouse antibodies (eBioscience). Nuclei were stained with 4′,6-diamidino-2-phenylindole (DAPI). Images were acquired using an Olympus fluorescence microscope. Four representative high-power field images were captured from each colon and processed using Olympus cellSens software.

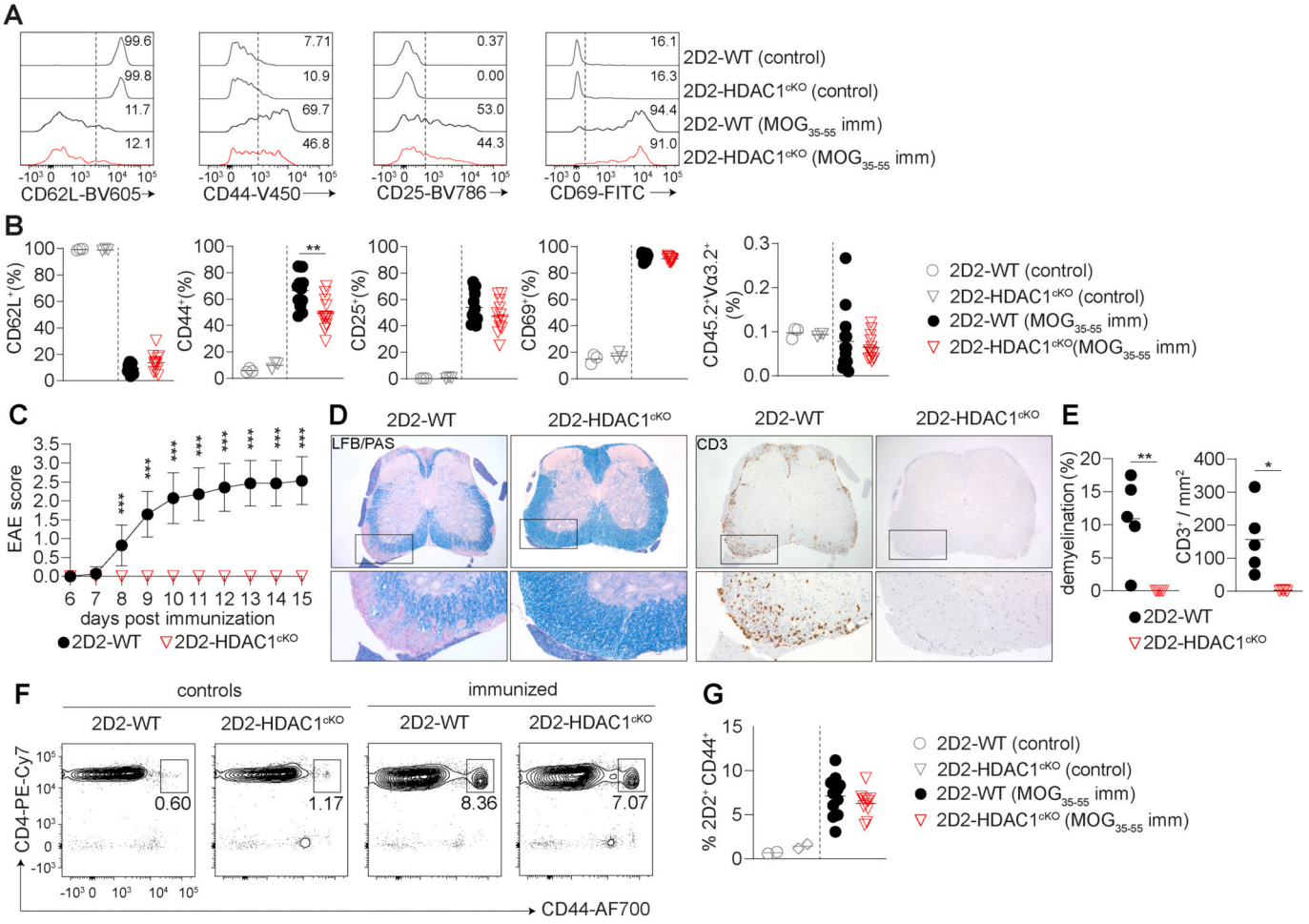

Fig. 1. 2D2-HDAC1^{cKO} mice are resistant to EAE induction despite efficient *in vivo* CD4$^+$ T cell priming. (a) Naïve 2D2-WT or 2D2-HDAC1^{cKO} $CD4^+$ T cells ($CD45.1^-CD45.2^+$) were transferred into recipient mice ($CD45.1^+CD45.2^+$) which were immunized with MOG_{35-55} peptide/CFA (MOG_{35-55} imm) on the next day. Two days later $CD45.2^+V\alpha3.2^+$ 2D2 T cells within draining lymph nodes were analyzed. Representative histograms show cell surface expression of CD62L, CD44, CD25 and CD69 on recovered $CD45.2^+V\alpha3.2^+$ 2D2 T cells. Controls are transferred naïve 2D2-WT or 2D2-HDAC1^{cKO} $CD4^+$ T cells isolated from recipient mice that were immunized with PBS/CFA. **(b)** Summary graphs depict percentages of cell surface markers on $CD45.2^+V\alpha3.2^+$ 2D2 T cells and percentage of $CD45.2^+V\alpha3.2^+$ 2D2 T cells in draining lymph nodes of mice that have been treated as described in **(a)**. **(c)** Clinical EAE disease score of 2D2-WT and 2D2-HDAC1^{cKO} mice following immunization with MOG_{35-55} peptide/CFA and injection of pertussis toxin on day 0 and day 2. **(d)** Brain sections of 2D2-WT and 2D2-HDAC1^{cKO} mice (day 15 post immunization) stained with LFB-PAS myelin for visualization of demyelinated areas (left two panels) and CD3 for detecting lymphocyte infiltration (right two panels). The lower panels show a magnification of the boxed areas. **(e)** Summary diagrams depict percentage of demyelination (left) and number of infiltrated $CD3^+$ cells per mm^2 (right). **(f)** Flow cytometry analysis of blood samples taken from 2D2-WT and 2D2-HDAC1^{cKO} mice on day 8 following EAE induction shows percentages of $2D2^+CD44^+$ cells in peripheral blood compared to non-immunized controls. **(g)** Dot plots show summary of $2D2^+CD44^+$ cells in peripheral blood on day 8 following EAE induction. Horizontal bars indicate the mean. *$p < 0.05$, **$p < 0.01$, ***$p < 0.001$ (unpaired two-tailed student's t-test). Differences that did not reach a statistically significant level (i.e., $p \geq 0.05$) are not indicated. Data are representative **(a,d,f)** or show summary of 12–13 **(b),** 14 **(c)**, 5 **(e)** and 11 **(g)** mice per group (except controls with 2–3 mice) analyzed in 3 **(b,c)** and 2 **(g)** independent experiments.

2.19. Data availability statement

RNA-seq data reported in this study have been deposited in the National Center for Biotechnology Information's Gene Expression Omnibus database under number GSE159705.

3. Results

3.1. In vivo activation and expansion of antigen-specific CD4$^+$ T cells is not impaired in the absence of HDAC1

We have previously shown that a conditional deletion of HDAC1 in T cells protects mice against the induction of EAE [21]. The cellular and molecular mechanism of how loss of HDAC1 protects against EAE remained elusive, although we ruled out several possibilities such as the presence of a hyper-suppressive CD25$^+$ regulatory T cell subset in HDAC1^{cKO} mice or that HDAC1^{cKO} CD4$^+$ T cells failed to differentiate *in vitro* into Th1 and Th17 cells [21–23]. However, loss of HDAC1 might affect the *in vivo* activation and expansion of CD4$^+$ T cells. To study whether the antigen-specific activation or expansion of CD4$^+$ T cells *in vivo* is altered in the absence of HDAC1, we crossed *Hdac1*$^{fl/fl}$ (designated as WT) and HDAC1^{cKO} mice to 2D2 TCR transgenic mice that express a TCR (formed by Vα3.2 and Vβ11) specific for the myelin oligodendrocyte glycoprotein peptide 35–55 (MOG_{35-55}) [25]. Naïve CD45.2$^+$ 2D2-WT (CD45.1$^-$CD45.2$^+$) or 2D2-HDAC1^{cKO} CD4$^+$ T cells (CD45.1$^-$CD45.2$^+$) were isolated from these mice and transferred i.v. into CD45.1$^+$CD45.2$^+$ recipient mice followed by MOG_{35-55}/CFA footpad immunization. Two days later, transferred (CD45.1$^-$CD45.2$^+$) CD4$^+$ T cells in draining lymph nodes (dLN), spleens and peripheral lymph nodes (pLN) were analyzed for early activation marker expression (Supplementary Fig. 1a). We observed an upregulation of CD25 and CD69 accompanied by a downregulation of CD62L to a similar extent in 2D2-HDAC1^{cKO} and 2D2-WT CD4$^+$ T cells within dLN (Fig. 1a and b). CD44 was also upregulated in 2D2-HDAC1^{cKO} T cells following activation, however to a lesser degree as compared to 2D2-WT T cells (Fig. 1a and b). A similar difference in CD44 upregulation was observed in splenic 2D2-HDAC1^{cKO} T cells (Supplementary Fig. 1b). However, the percentages and absolute numbers of 2D2-HDAC1^{cKO} CD4$^+$ T cells were comparable to 2D2-WT CD4$^+$ T cells in all organs examined (Fig. 1b, Supplementary Fig. 1c). To study the expansion of transferred 2D2-WT and 2D2-HDAC1^{cKO} CD4$^+$ T cells, we analyzed dLNs, spleens and pLNs 4 days after MOG_{35-55}/CFA footpad immunization and assessed cell numbers and activation marker expression (Supplementary Fig. 2a). Both 2D2-HDAC1^{cKO} and 2D2-WT T cells expanded to a similar extent as indicated by comparable percentages and cell numbers (Supplementary Fig. 2b). At this time point CD62L, CD25 and CD69 were already efficiently downregulated in both 2D2-HDAC1^{cKO} and 2D2-WT T cells (Supplementary Figs. 2c and d). Whereas almost all transferred dLN 2D2-WT T cells upregulated CD44, only approx. 80% of 2D2-HDAC1^{cKO} T cells expressed CD44. Similar results were obtained in the spleen and pLNs (Supplementary Fig. 2d). Taken together, despite differences in the upregulation of CD44 expression, these data exclude the possibility that an impaired activation and/or expansion of antigen-specific CD4$^+$ T cells would cause protection of HDAC1^{cKO} mice from EAE.

Since both 2D2-WT and 2D2-HDAC1^{cKO} CD4$^+$ T cells efficiently expanded *in vivo* upon MOG/CFA immunization, we next investigated whether MOG_{33-55} antigen-specificity in 2D2-HDAC1^{cKO} mice restored disease susceptibility in the absence of HDAC1. Upon immunization with MOG_{35-55}/CFA to induce disease 2D2-WT mice developed clinical signs of EAE around day 8 peaking at around day 12. In contrast, 2D2-HDAC1^{cKO} mice were fully protected from developing EAE (Fig. 1c). CNS T cell infiltrates were readily detected in 2D2-WT mice and this was accompanied by severely demyelinated brain regions (Fig. 1d and e). In contrast, immunized 2D2-HDAC1^{cKO} mice were lacking T cell infiltrates in both the brain and spinal cords, as previously observed in HDAC1^{cKO} mice [21] (Fig. 1d and e) and there were no signs of demyelination in 2D2-HDAC1^{cKO} mice (Fig. 1d and e). A comprehensive flow cytometry analysis of peripheral blood from 2D2-WT and 2D2-HDAC1^{cKO} mice 8 days after disease induction indicated comparable frequencies of activated CD44$^+$ transgenic 2D2 CD4$^+$ T cells (Fig. 1f and g), in line with our data showing similar activation and expansion of transferred 2D2-WT and 2D2-HDAC1^{cKO} CD4$^+$ T cells (Fig. 1a and b, Supplementary Figs. 1 and 2). Similarly, at the peak of disease in 2D2-WT mice (day 15) the frequencies of effector/memory CD62L$^-$CD44$^+$CD4$^+$ T cell subsets within the total CD4$^+$ T cell population in the spleen were also comparable in 2D2-WT and 2D2-HDAC1^{cKO} mice (Supplementary Figs. 3a and b). Upon PMA/Ionomycin restimulation, frequencies of IL-17A$^+$, IFNγ$^+$IL-17A$^+$ and GM-CSF$^+$ 2D2-TCR$^+$ CD4$^+$ T cells were comparable in 2D2-HDAC1^{cKO} and 2D2-WT splenocytes whereas percentages of IFNγ, IL-2 and TNFα single-producing 2D2 CD4$^+$ T cells were increased in 2D2-HDAC1^{cKO} compared to 2D2-WT splenocytes (Supplementary Figs. 3c and d). This indicates that lack of HDAC1 in 2D2 CD4$^+$ T cells does not impair their differentiation into Th1/Th17 cells *in vivo*. Furthermore, these data indicate that the cause of EAE protection in HDAC1^{cKO} mice cannot be explained by a lack of T cells reactive to MOG_{35-55} peptide which might have resulted from alterations in the T cell repertoire.

3.2. Transcriptome changes in HDAC1^{cKO} CD4$^+$ T cells upon in vivo activation

Although there were no differences in activation and expansion of 2D2-WT and 2D2-HDAC1^{cKO} CD4$^+$ T cells on day 4 post-immunization (Supplementary Fig. 2), we reasoned that *in vivo*-activated HDAC1^{cKO} CD4$^+$ T cells in the dLN might already display transcriptional differences that reveal why these cells fail to induce EAE. Therefore, we next analyzed the transcriptome of *in vivo* activated antigen-specific HDAC1^{cKO} CD4$^+$ T cells using RNA-sequencing (RNA-seq). To this end, either 2D2-WT or 2D2-HDAC1^{cKO} CD4$^+$ T cells (CD45.1$^-$CD45.2$^+$) were transferred into CD45.1$^+$CD45.2$^+$ mice followed by MOG_{35-55}/CFA immunization of the recipient mice. Subsequently, MOG_{35-55}-specific CD4$^+$ T cells were isolated on day 4 post-immunization and subjected to low-input Smart-seq2 RNA-sequencing. In 2D2-HDAC1^{cKO} CD4$^+$ T cells 887 genes were downregulated and 928 genes were upregulated in comparison to 2D2-WT CD4$^+$ T cells (Fig. 2a). Ingenuity pathway analysis revealed "leukocyte extravasation signaling" as one of the top five dysregulated canonical pathways (Fig. 2b) and displayed a downregulation in 2D2-HDAC1^{cKO} CD4$^+$ T cells. Since our previous results in mixed WT and HDAC1^{cKO} BM chimeric mice showed that predominantly WT and only a small fraction of HDAC1^{cKO} CD4$^+$ T cells infiltrated the CNS in an EAE disease setting and thus suggested that the migration of HDAC1-deficient CD4$^+$ T cells might be impaired [21], we analyzed this pathway in more detail. Several genes involved in regulating rolling and arrest of T cells to endothelial cells were expressed at a lower levels in the absence of HDAC1, among them members of the selectin ligand family, such as *Selplg* and *Spn*, the integrin family members *Itgal* and *Itgb2* (encoding for CD11a and CD18, the two chains forming LFA-1) as well as *Itgb7* (Fig. 2c and d). Moreover, *Actb, Actn2, Msn, Vasp and Wipf1*, which are known to sustain leukocyte shape remodeling and polarity upon selectin and integrin activation in the context of transendothelial migration [36], were significantly downregulated in 2D2-HDAC1^{cKO} CD4$^+$ T cells (Fig. 2c). Furthermore, expression of *Fut7*, *Gcnt1* and *Tpst2*, genes encoding enzymes required in the core 2 O-Glycan synthesis pathways and hence in the generation of functional glycosylated selectin ligands such as PSGL-1 and CD43, was also down in HDAC1-deficient CD4$^+$ T cells (Fig. 2d). Deletion of HDAC1 in CD4$^+$ T cells hence results in transcriptional changes which may affect CD4$^+$ T cell trafficking.

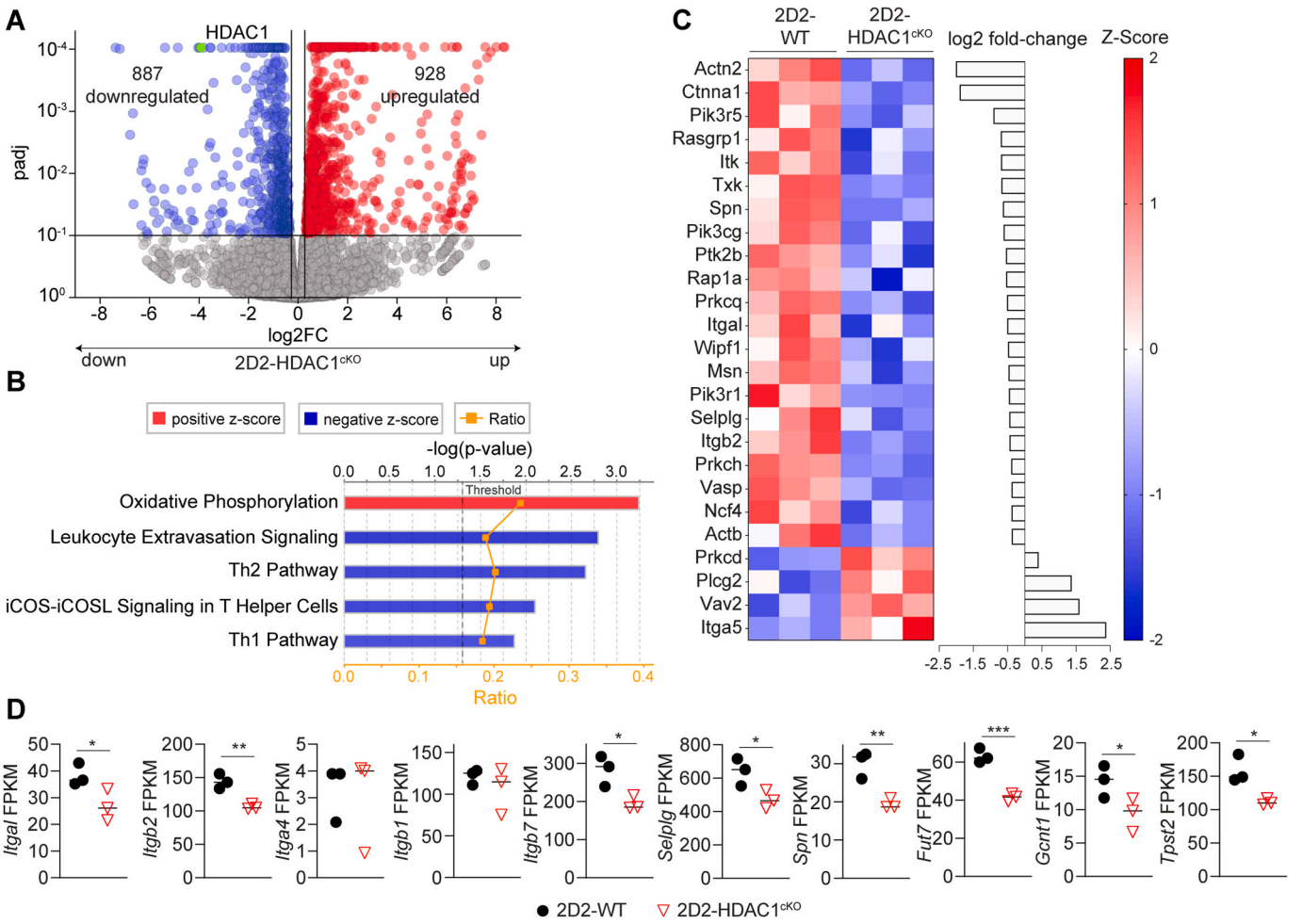

Fig. 2. Reduced expression of genes associated with leukocyte extravasation signaling in *in vivo* activated 2D2-HDAC1^{cKO} CD4$^+$ T cells. 2D2-WT and 2D2-HDAC1^{cKO} CD4$^+$ T cells (CD45.2$^+$) were isolated 4 days after transfer of naïve cells into recipient mice (CD45.1$^+$) and activation via MOG_{35-55}/CFA immunization. Sorted viable 2D2$^+$CD45.2$^+$ cells from three independent batches were subjected to low-input Smart-seq2 sequencing. **(a)** Volcano plot depicts the comparison of gene expression profiles between 2D2-WT and 2D2-HDAC1^{cKO} CD4$^+$ T cells. On the x-axis the $\log_2$ fold change is plotted, the y-axis indicates adjusted p-values (padj, $-\log_{10}$). 887 genes are downregulated and 928 upregulated in 2D2-HDAC1^{cKO} CD4$^+$ T cells compared to 2D2-WT CD4$^+$ T cells (FDR $\leq$ 0.05). **(b)** Diagram showing the top five dysregulated canonical pathways ($-2 \geq$ Z score ≥ 2; $p \leq 0.05$) revealed by Ingenuity Pathway Analysis predicted to be up- (positive z-score, red) or downregulated (negative z-score, blue) in 2D2-HDAC1^{cKO} CD4$^+$ T cells. Pathways are described on the y-axis. The x-axis indicates the –log of the p-value (threshold = 0.05). Orange points on each pathway depict the ratio of genes within one pathway that are dysregulated. **(c)** Heatmap of gene expression values depicting changes in gene expression between 2D2-WT and 2D2-HDAC1^{cKO} CD4$^+$ T cells of significantly dysregulated genes (FPKM value $\geq$ 0.5, p-value $\leq$ 0.05) within the leukocyte extravasation pathway. Triplicate values are depicted in columns and gene names are represented in rows. The $\log_2$ fold change for each gene is represented by the bar diagram and Z-scores are indicated by colour code. **(d)** Diagrams depict expression values (shown as fragments per kilobase of transcript per million mapped reads; FPKM) of selected genes in *in vivo* activated 2D2-WT and 2D2-HDAC1^{cKO} CD4$^+$ T cells as determined by RNA-seq. Each symbol represents one biological replicate. Horizontal bars indicate the mean. *p < 0.05, **p < 0.01, ***p < 0.001 (unpaired two-tailed student's t-test). (For interpretation of the references to colour in this figure legend, the reader is referred to the Web version of this article.)

3.3. HDAC1-deficient CD4$^+$ T cells display impaired adhesion to brain endothelial cells

Circulating encephalitogenic effector CD4$^+$ T cells have to cross the brain barriers to reach the CNS and to trigger clinical EAE [2,4]. Since HDAC1^{cKO} CD4$^+$ T cells showed lower expression of the subunits of LFA-1 but not of VLA-4 (Fig. 2d), and since the entry of Th17 cells into the CNS is dependent on the expression of LFA-1 [37], we used a microscopy-based *in vitro* assay to test the impact of ICAM-1 binding on Th17 cells in the absence of HDAC1. WT and HDAC1^{cKO} Th17 cells were seeded on ICAM-1-coated surfaces and allowed to adhere for 30 min at 37 °C. Following incubation, the cells were fixed and stained with Phalloidin-AF488 conjugate to determine F-actin levels and distribution. Quantification of cell area and F-actin levels revealed a significant increase in cell spreading (approx. 10%) and F-actin levels (approx. 25%) at the cell bottom in HDAC1^{cKO} Th17 cells in comparison to WT Th17 cells (Fig. 3a and b), indicating altered LFA-1-dependent cytoskeletal responses in the absence of HDAC1. To study whether the morphological changes in response to ICAM-1 binding are linked with an altered migratory behavior of HDAC1^{cKO} T cells we analyzed random migration velocities of CXCL-12-primed WT and HDAC1^{cKO} Th17 cells on ICAM-1 coated surfaces [28]. Live cell imaging of differentially labelled WT and HDAC1^{cKO} Th17 cells revealed a 10% increase in average cell speed of HDAC1^{cKO} Th17 cells as compared to WT Th17 cells (Fig. 3c, Supplementary Fig. 4a, Supplementary movie 1) suggesting that HDAC1^{cKO} Th17 cells are biased towards an enhanced migratory behavior.

LFA-1:ICAM-1 receptor-ligand interactions are important for adhesion to primary mouse brain microvascular endothelial cells (pMBMECs) [38]. To elucidate whether the deviations in the transcriptome and the altered response to ICAM-1 correlated with changes in the ability of HDAC1-deficient effector CD4$^+$ T cells to cross tight endothelial barriers, we performed transwell migration assays. *In vitro*-generated WT

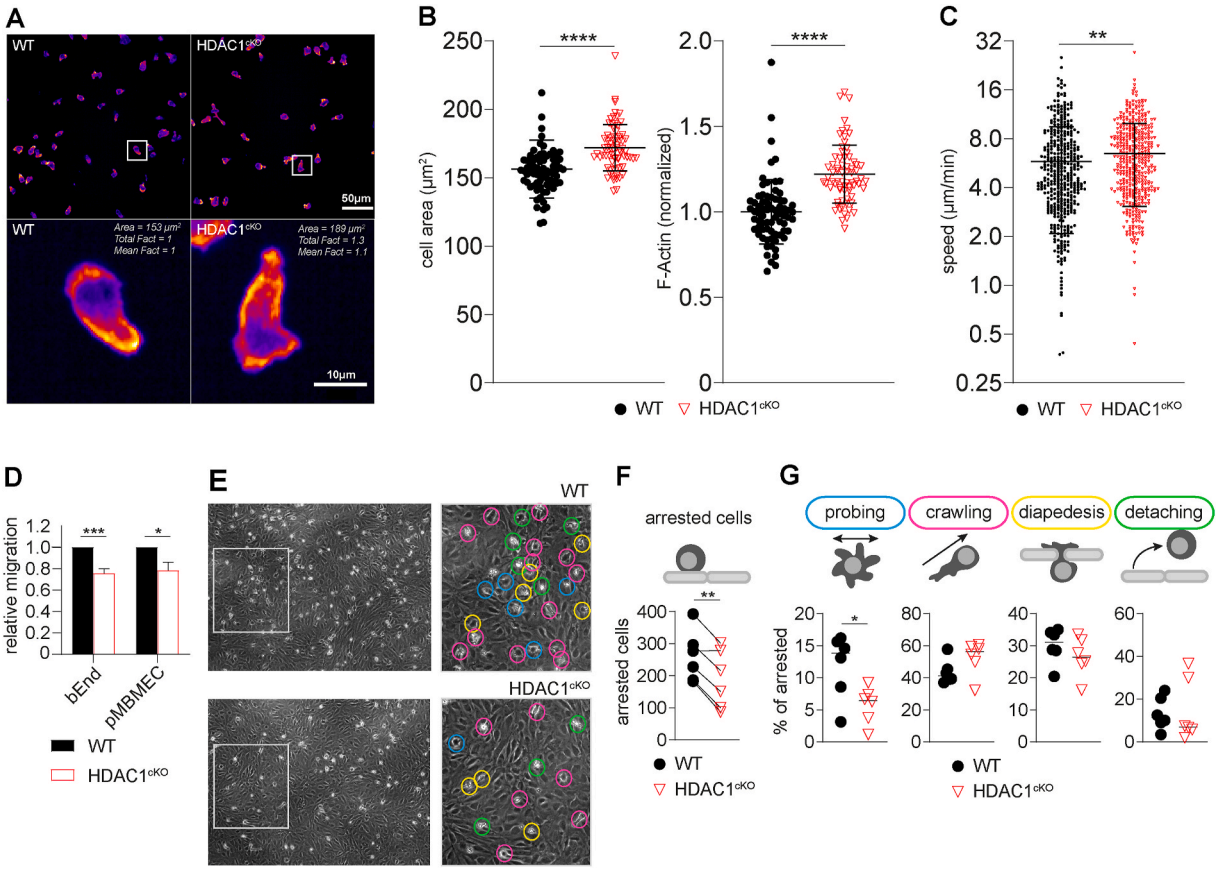

Fig. 3. HDAC1 deficiency in Th17 cells affects arrest to endothelial cells under flow and cell speed on ICAM-1-coated surfaces. (a) WT and HDAC1^{cKO} Th17 cells were deposited on ICAM-1-coated surfaces and analyzed for cell spreading (cell area) as well as F-actin content (normalized F-actin) by immunofluorescent staining. **(b)** Dot plots show summary of cell spreading (cell area) and F-actin content of WT and HDAC1^{cKO} Th17 cells on ICAM-1-coated surfaces (n = 71 for WT and 72 for HDAC1^{cKO}). **(c)** WT and HDAC1^{cKO} Th17 cell migration speed (log2 scale) on ICAM-1 and CXCL-12-coated surfaces. Each symbol represents the mean speed of a single cell (n = 416 for WT and 420 for HDAC1^{cKO}). **(d)** Bar diagrams show diapedesis rate of HDAC1^{cKO} Th17 cells relative to WT Th17 cells across bEnd5 (left side) and pMBMEC cells (right side) seeded on 5 µm transwell inserts. **(e)** Picture depicts field of view of WT (upper panels) and HDAC1^{cKO} (lower panels) Th17 cells arrested on IL-1β stimulated pMBMECs under physiological flow conditions (1.5 dyn/cm^2). The right panels show a magnification of the boxed areas and attached cells are circled. Color codes mark the respective post-arrest behavior (probing: blue, crawling: pink, diapedesis: yellow, detaching: green) determined by manual tracking as exemplified in supplementary movie 4. **(f)** Diagram summarizes the number of arrested WT and HDAC1^{cKO} Th17 cells per field of view as shown in **(e)**. **(g)** Post-arrest behavior of WT and HDAC1^{cKO} Th17 cells on pMBMECs is categorized as probing, crawling, diapedesis and detaching and shown as percent of arrested cells per field of view. Horizontal lines indicate the mean. Statistical analysis was performed using an unpaired two-tailed student's t-test **(b,c,d)** and a paired two-tailed student's t-tests **(f,g)**. *p < 0.05, **p < 0.01, ***p < 0.001, ****p < 0.0001. Data are representative **(a,e)** or show the summary of 3–5 **(d)**, 6 **(f,g)** and 2 **(a,b)** independent experiments. (For interpretation of the references to colour in this figure legend, the reader is referred to the Web version of this article.)

and HDAC1^{cKO} Th17 cells were mixed at a 1:1 ratio and assessed for their transendothelial migration ability across monolayers of the brain endothelioma cell line bEnd.5 or pMBMEC layers seeded on porous filter membranes (Fig. 3d). HDAC1^{cKO} Th17 cells showed, compared to WT Th17 cells, a significantly reduced ability to cross these endothelial monolayers (Fig. 3d). Of note, chemotaxis of HDAC1^{cKO} Th17 cells towards the chemokines CCL20 and CCL21 across porous filer membranes without an endothelial barrier was 2-fold enhanced compared to WT Th17 cells (Supplementary Fig. 4b). These data indicate that HDAC1-deficient CD4$^+$ T cells display altered motility properties in a context-dependent manner and that their reduced ability to migrate across endothelial cell layers is in line with the downregulation of genes associated with leukocyte extravasation.

Next, we aimed to more physiologically recapitulate the multi-step migration process of T cells across the BBB. We therefore studied CD4$^+$ T cell migration on and across pMBMEC monolayers under physiological flow conditions by live cell imaging [27]. pMBMEC monolayers were pre-activated with IL-1β to induce high-level expression of ICAM-1 and VCAM-1, which results in firm LFA-1- and VLA-4-mediated arrest of activated T cells on the pMBMEC monoayers under flow [38]. The number of HDAC1^{cKO} Th17 cells arresting on IL-1β-treated pMBMECs was significantly lower compared to WT Th17 cells (Fig. 3e and f, Supplementary movie 2). A similar effect was also observed on TNFα-treated pMBMEC monolayers (Supplementary Fig. 4c, Supplementary movie 3). The post-arrest behavior of those CD4$^+$ T cells that arrested to monolayers under flow conditions can be subdivided into at least 4 categories: probing for sites permissive for diapedesis, crawling, diapedesis and detaching (Supplementary movie 4) [39,40]. While there were no differences between WT and HDAC1^{cKO} Th17 cells in their rate of detachment or their abilities to crawl on and cross pMBMEC monolayers (Fig. 3g, Supplementary Fig. 4d), we observed a 50% reduction in the fraction of HDAC1^{cKO} Th17 cells probing to breach the pMBMEC barrier when compared to control WT Th17 cells (Fig. 3g). Taken together, these data suggest that impaired transendothelial migration of HDAC1^{cKO} Th17 cells is a consequence of their reduced ability to arrest to endothelial cells.

3.4. Impaired homing of HDAC1-deficient CD4$^+$ T cells to the intestinal epithelium and lamina propria

Our results implicate LFA-1-dependent cellular processes or the lack thereof in HDAC1^{cKO} Th17 cells as being instrumental in

transendothelial migration. We therefore explored whether migration across barriers also depends on HDAC1 in other models of auto-inflammatory diseases, in which LFA-1 function appears critical. LFA-1 expression on activated CD4$^+$ T cells is essential for proper homing of effector Th cells into intestinal tissues in an adoptive T cell transfer colitis model [41–44]. Since LFA-1 surface levels are reduced in activated HDAC1^{cKO} CD4$^+$ T cells *in vivo*, we tested whether HDAC1-deficient CD4$^+$ T cells are able to home to intestinal organs and to induce colitis. WT and HDAC1^{cKO} CD4$^+$ T cells were transferred into B and T cell-deficient *Rag2*$^{-/-}$ mice and recipient mice were monitored over a period of 6 weeks for weight loss followed by histological and flow cytometry analysis of intestinal tissues. *Rag2*$^{-/-}$ mice that had received WT CD4$^+$ T cells displayed a loss of around 10% of their initial body weight at week 6 (Fig. 4a), which was not observed in *Rag2*$^{-/-}$ mice without T cell transfer or after transfer of HDAC1^{cKO} CD4$^+$ T cells (Fig. 4a). Body weight reduction of *Rag2*$^{-/-}$ mice that had received WT CD4$^+$ T cells also correlated with severe crypt damage and T cell infiltration into the colon (Fig. 4b), which was not detectable in mice receiving HDAC1^{cKO} CD4$^+$ T cells (Fig. 4b). Furthermore, HDAC1^{cKO} CD4$^+$ T cell infiltration into the colon was diminished and HDAC1^{cKO} IEL were almost absent in comparison to *Rag2*$^{-/-}$ mice receiving WT CD4$^+$ T cells (Fig. 4b). A comprehensive flow cytometry analysis of peripheral and intestinal organs showed that the percentage of HDAC1^{cKO} CD4$^+$ T cells was only mildly reduced in the spleen (1.8-fold) and mesenteric lymph nodes (mLNs) (1.2-fold) of recipient *Rag2*$^{-/-}$ mice. Furthermore, reduced percentages in the spleen but not in mLNs correlated with reduced splenic HDAC1^{cKO} CD4$^+$ T cell numbers (Fig. 4c and d upper panels). In contrast to the mild reduction in T cell frequencies observed in the spleen and mLNs, the percentage of small intestinal lamina propria (SI-LP) lymphocytes was severely (>3-fold) decreased in *Rag2*$^{-/-}$ mice receiving HDAC1^{cKO} CD4$^+$ T cells. The reduction in HDAC1-deficient CD4$^+$ T cells was even more pronounced for small intestinal intraepithelial lymphocyte (SI-IEL) subsets with only 5% HDAC1^{cKO} IELs compared to 75% WT IELs (Fig. 4d, lower panels). This also corresponded with strongly diminished numbers of SI-LP and SI-IEL HDAC1^{cKO} CD4$^+$ T cells (Fig. 4d, lower panels). These results suggest that homing of HDAC1^{cKO} CD4$^+$ T cells to mLNs is *per se* not impaired, whereas trafficking of these cells to the lamina propria and intestinal epithelium are markedly affected. Furthermore, *ex vivo* stimulation of isolated T cells revealed that the percentage of the IFNγ$^+$IL-17A$^-$ population was slightly but significantly reduced by 10–20% in HDAC1^{cKO} CD4$^+$ T cells in the spleen, mLNs as well as in the

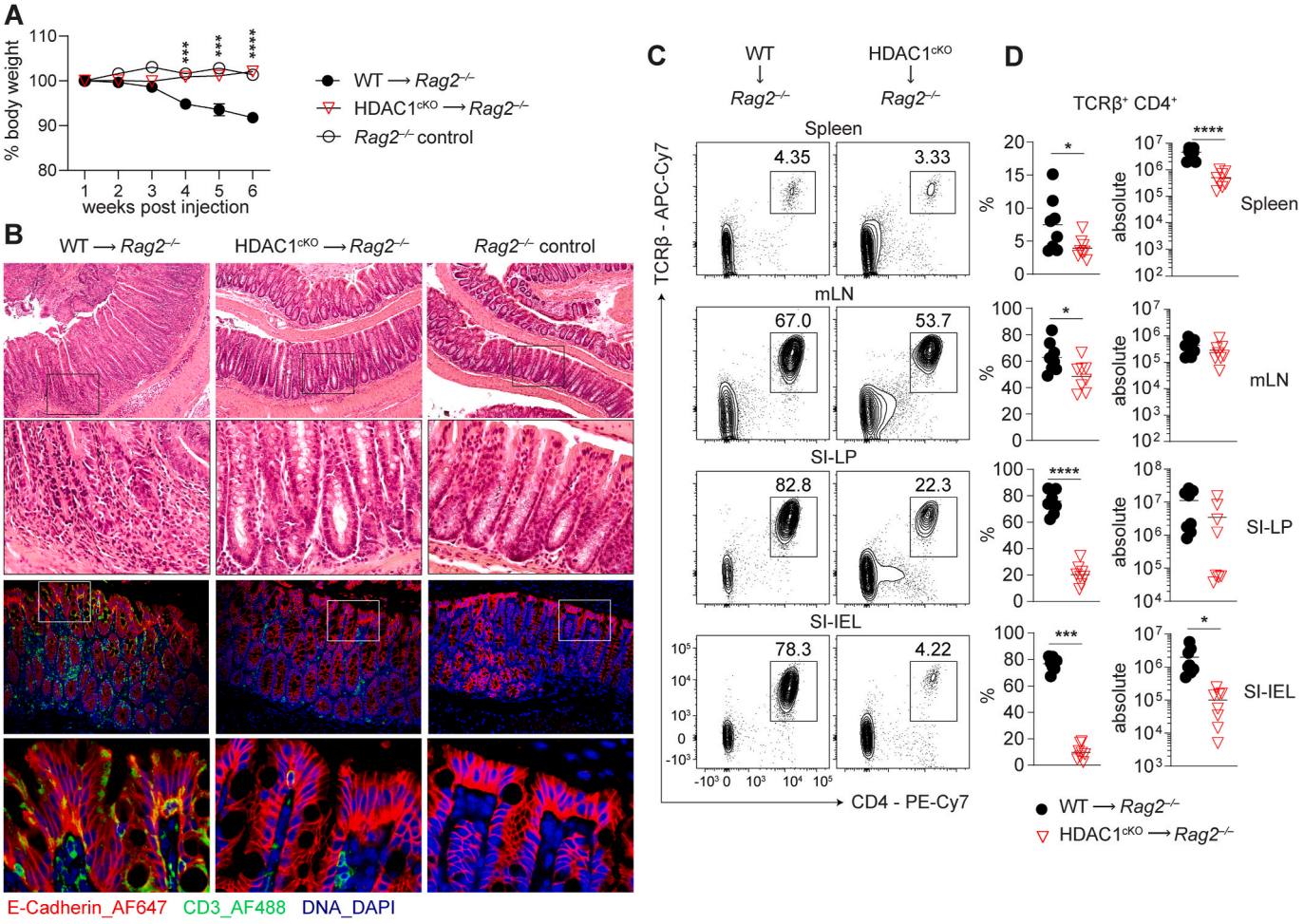

Fig. 4. HDAC1 deficiency in CD4$^+$ T cells ameliorates T cell transfer colitis in *Rag2*$^{-/-}$ recipient mice. (a) Weight scores in percent of initial body weight during the course of colitis induction via naïve WT or HDAC1^{cKO} CD4$^+$ T cell transfer into *Rag2*$^{-/-}$ recipient mice are shown. Control *Rag2*$^{-/-}$ mice did not receive any cells. **(b)** 6 weeks post transfer colon swiss rolls were processed for immunofluorescence staining of E-cadherin (red), CD3 (turquoise) and nuclei (DAPI, blue). **(c)** Representative contour plots show percentages of WT and HDAC1^{cKO} TCRβ$^+$CD4$^+$ cells in spleen, mesenteric lymph nodes (mLN), small intestinal lamina propria (SI-LP) and small intestinal intraepithelial lymphocytes (SI-IEL) isolated from *Rag2*$^{-/-}$ recipient mice 6 weeks post transfer. Numbers indicate the percentage of cells in the defined region. **(d)** Diagrams show summary of percentages and absolute numbers of TCRβ$^+$CD4$^+$ cells in indicated organs. Each dot represents one recipient mouse. Horizontal bars indicate the mean. Data are representative **(b,c)** or show a summary of two independent experiments **(a,d)** with 4 mice per group within each experiment. *p < 0.05, **p < 0.01, ***p < 0.001, ****p < 0.0001 (unpaired two-tailed student's t-test). (For interpretation of the references to colour in this figure legend, the reader is referred to the Web version of this article.)

SI-LP, whereas the percentage of IFNγ^{-}IL-17A^{+} HDAC1^{cKO} CD4^{+} T cells was approximately 2-fold increased in splenic and SI-LP lymphocytes (Supplementary Figs. 5a and b). There was no difference in the fraction of IFNγ and IL-17A double-producers (Supplementary Figs. 5a and b). These data demonstrate that there are no major alterations in effector function of HDAC1-deficient CD4^{+} T cells and indicate that the reduced ability of HDAC1^{cKO} CD4^{+} T cells to trigger colitis is likely due to impaired intestinal homing.

To further investigate features associated with the tissue homing of adoptively transferred HDAC1-deficient CD4^{+} T cells, we assessed the surface expression levels of the two LFA-1 chains CD11a and CD18. Both were significantly reduced (by 40% and 30%, respectively) in splenic HDAC1^{cKO} CD4^{+} T cells of *Rag2*$^{-/-}$ recipient mice and CD11a expression was also reduced (by 25%) on HDAC1^{cKO} CD4^{+} T cells in mLNs in comparison to WT CD4^{+} T cells (Fig. 5a and b). Interestingly, there was no difference in CD18 and only a mild decrease in CD11a expression on HDAC1^{cKO} SI-IELs compared to WT SI-IELs (Fig. 5a and b), suggesting that HDAC1^{cKO} CD4^{+} T cells which had acquired high LFA-1 expression were able to home to intestinal tissues. The recruitment of effector T cells to inflamed tissues is also regulated via the binding of selectin ligands CD162 (PSGL-1), CD44 and CD43 expressed on activated T cells to E- and P-selectin expressed on endothelial cells [45]. CD43 was downregulated in HDAC1^{cKO} CD4^{+} T cells to about 55–70% of the levels seen in WT CD4^{+} T cells in all organs analyzed and CD162 and CD44 expression levels were markedly reduced in mLN HDAC1^{cKO} CD4^{+} T cells and SI-IELs (Fig. 5c and d). These results indicate that HDAC1 is a

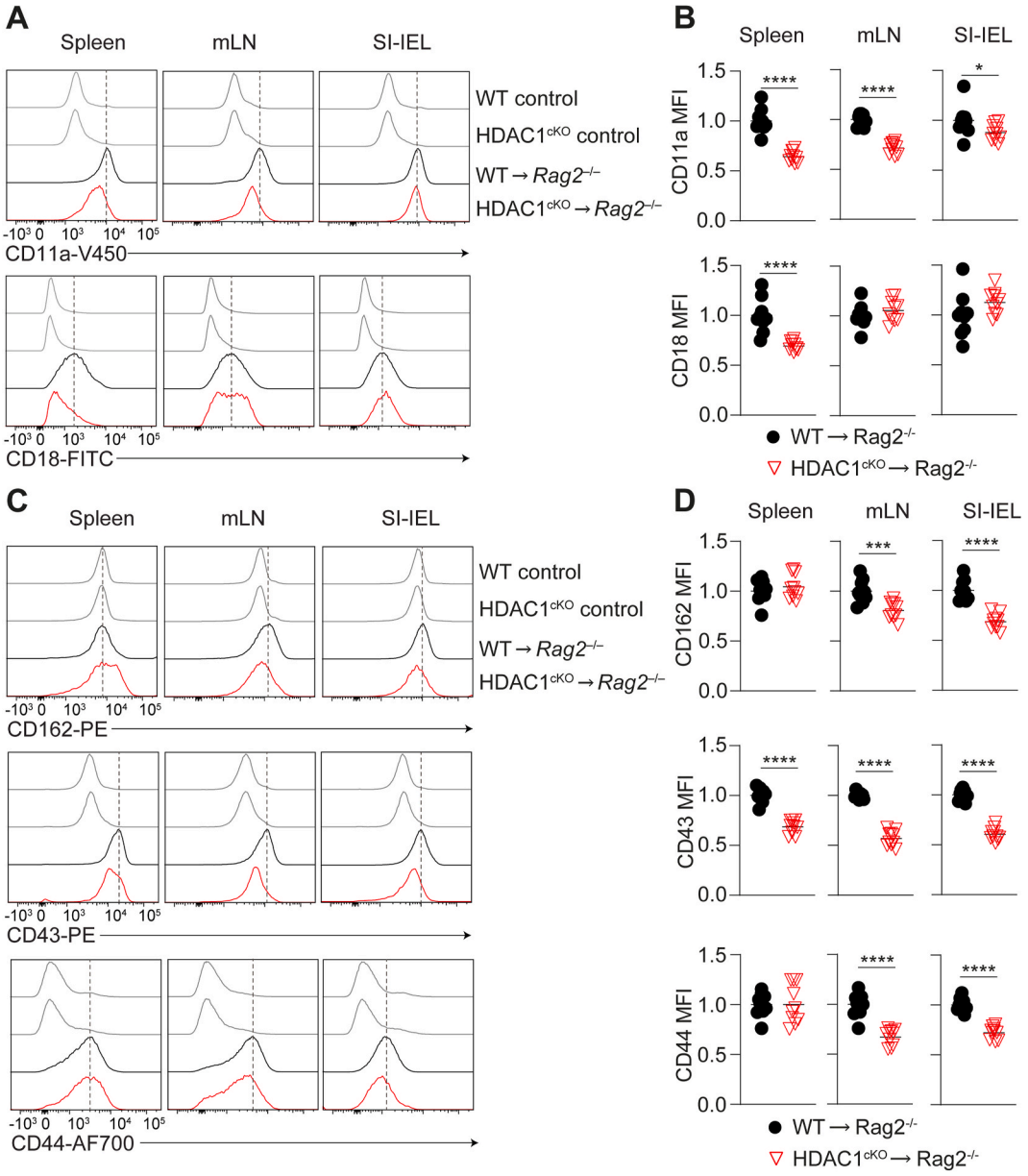

Fig. 5. Reduced expression of LFA-1 and selectin ligands in the absence of HDAC1 is associated with impaired homing of CD4^{+} T cells into intestinal organs. (a) Representative histograms show cell surface expression of CD11a and CD18 on TCRβ^{+}CD4^{+} cells isolated from spleen, mesenteric lymph nodes (mLN) and small intestinal intraepithelial lymphocytes (SI-IEL) recovered from *Rag2*$^{-/-}$ recipient mice 6 weeks post transfer. As control, CD11a and CD18 expression on naïve CD4^{+} T cells in WT and HDAC1^{cKO} mice is shown. **(b)** Summary graph depicts normalized geometric mean fluorescence intensity (MFI) of cell surface markers CD11a and CD18. **(c)** Representative histograms show cell surface expression of CD162, CD44 and CD43 of TCRβ^{+}CD4^{+} cells in spleen, mesenteric lymph nodes (mLN) and small intestinal intraepithelial lymphocytes (SI-IEL) recovered from *Rag2*$^{-/-}$ recipient mice 6 weeks post transfer. **(d)** Graphs summarize normalized geometric MFI of cell surface markers CD162, CD44 and CD43. **(b,d)** Horizontal bars indicate the mean. *p < 0.05, **p < 0.01, ***p < 0.001, ****p < 0.0001 (unpaired two-tailed student's t-test). Data are representative **(a,c)** or show summary of 12–13 **(b,d)** mice per group analyzed in 3 **(b,d)** independent experiments.

key regulatory factor that controls integrin as well as selectin ligand expression and suggest that their reduced expression in the absence of HDAC1 results in altered trafficking of $CD4^+$ T cells.

4. Discussion

We have previously demonstrated that a T cell-specific deletion of HDAC1 protects mice from developing EAE [21], however the cellular and molecular mechanism have remained elusive. In this study, we demonstrate that HDAC1 in $CD4^+$ T cells is instrumental for the proper expression of genes associated with leukocyte extravasation, for the regulation of cell morphology and migration on surfaces coated with the integrin LFA-1 ligand ICAM-1, and for adhesion of $CD4^+$ T cells to brain endothelial cells required for transendothelial migration. These processes were impaired in the absence of HDAC1, thus providing a mechanistic explanation of why $HDAC1^{cKO}$ mice are resistant to EAE. Further, our study revealed that $HDAC1^{cKO}$ $CD4^+$ T cells failed to induce disease in an adoptive $CD4^+$ T cell transfer colitis model. This correlated with a severe reduction of intestinal and colonic $HDAC1^{cKO}$ $CD4^+$ T cells but not of splenic and mLN $HDAC1^{cKO}$ $CD4^+$ T cells upon transfer, indicating impaired homing to intestinal tissues. Our data suggest a key role for HDAC1 in regulating T cell trafficking into tissues and thus in the control of T cell-mediated inflammation.

Several mechanisms can be envisaged of why $HDAC1^{cKO}$ mice are protected from EAE, such as $CD4^+$ T cell activation and expansion defects, a failure in Th1/Th17 differentiation as well as the inability of effector Th cells to migrate into the CNS. An important finding of our study was that 2D2 TCR transgenic $HDAC1^{cKO}$ mice were resistant to EAE induction despite normal activation and *in vivo* expansion of MOG_{33-35}-specific HDAC1-deficient $CD4^+$ T cells. These data rule out the possibility that alterations in the $CD4^+$ T cell repertoire and/or activation defects might result in deficient clonal expansion of MOG-specific T cells recognizing disease-inducing epitopes in $HDAC1^{cKO}$ mice. Together with our previous observation that Th1/Th17 differentiation is not impaired in the absence of HDAC1 [21,23], these results strongly suggest that processes other than $CD4^+$ T cell activation, expansion and Th subset differentiation are affected by the loss of HDAC1.

Effector $CD4^+$ T cell trafficking into the CNS is key for the induction of EAE and comprises several steps that include capture/rolling, integrin activation, arrest, crawling and diapedesis across the endothelial layer [46,47]. Our transcriptome analysis of *in vivo* activated 2D2-$HDAC1^{cKO}$ $CD4^+$ T cells revealed a downregulation of genes controlling leukocyte extravasation, including *Itgal* and *Itgb2* which encode for the LFA-1 subunits CD11a and CD18. The interaction of LFA-1 expressed on activated T cells with ICAM-1 and ICAM-2 expressed on activated vascular endothelium is crucial for cell shape, arrest and crawling of T cells [48,49] and Th17 cells rely on LFA-1 for efficient CNS infiltration [37]. Moreover, blockade of LFA-1 affects the motility of Th1 and Th17 cells at disease peak, and intrathecal injection of an anti-LFA-1 blocking antibody at the onset of EAE disease inhibits disease progression [50]. Since we also observed reduced expression of cytoskeletal genes required for cell polarization such as *Actb*, *Actn2* and *Msn*, we propose that reduced LFA-1 levels and potentially impaired LFA-1 downstream signaling results in a diminished adhesion to brain endothelial cell layers and hence impaired extravasation of HDAC1-deficient $CD4^+$ T cells into the CNS. More direct evidence to support our hypothesis that LFA-1-dependent cellular responses are altered was obtained from the finding that $HDAC1^{cKO}$ $CD4^+$ T cells displayed an altered cell shape upon binding to ICAM-1 as well as a faster random movement velocity on ICAM-1-coated glass slides. Furthermore, *in vitro*-generated $HDAC1^{cKO}$ Th17 cells were impaired in arresting on activated primary mouse brain microvascular endothelial cells under physiological flow as well as in crossing endothelial barriers. These processes were shown to be regulated, amongst others, by binding of LFA-1 to its ligands ICAM-1 and ICAM-2 [16,39,51–53]. Of note, the reduced probing frequency of $HDAC1^{cKO}$ Th17 cells under flow might contribute to the overall reduction in diapedesis and extravasation. Protrusions formed by T cells during probing have been shown to serve as mechanosenors for endothelial stiffness allowing for cell to breach endothelial barriers [54–56] and it has been proposed that shear forces exerted on high-affinity LFA-1 trigger adhesive and invasive filopodia at apical endothelial surfaces [51]. Thus, several LFA-1-dependent processes are crucially affected by loss of HDAC1.

Our data also suggest that HDAC1 regulates other steps of $CD4^+$ T cell migration in addition to the adhesion phase. Selectins play a key role in mediating capture/rolling of T cells on endothelial cells in inflamed tissues via their interaction with glycosylated selectin ligands expressed on T cells [57]. Our transcriptome data revealed a lower expression of several selectin ligand genes in $HDAC1^{cKO}$ $CD4^+$ T cells such as *Spn* (encoding for Leucosialin/CD43) and *Selplg* (encoding the P-selectin ligand CD162), which have been shown to mediate CNS homing in EAE [58–61]. Furthermore, several genes encoding for enzymes involved in the core 2 O-linked glycosylation of selectin ligands [57] were expressed at lower levels in $HDAC1^{cKO}$ $CD4^+$ T cells, which potentially might affect the interaction of selectin-ligands with selectins. We also observed reduced CD44 expression levels on *in vivo* activated $HDAC1^{cKO}$ $CD4^+$ T cells. CD44 binds to E-selectin and hyaluronan, thereby regulating cell adhesion to endothelial cells and migration within extracellular matrices [62–66]. Since blocking CD44 *in vivo* has been shown to ameliorate EAE and other autoinflammatory diseases [67–69], the inefficient upregulation of CD44 in the absence of HDAC1 might also contribute to disease protection. Together, these data suggest that in addition to $CD4^+$ T cell adhesion defects also potential alterations in $CD4^+$ T cell capture/rolling are likely to contribute to the dysregulated migration of $HDAC1^{cKO}$ $CD4^+$ T cells and as a consequence to the protection of $HDAC1^{cKO}$ mice against EAE. Whether the observed downregulation of genes associated with leukocyte extravasation is due to a direct effect of HDAC1 on the chromatin state of particular gene loci (by deacetylating histones) or indirect effect (e.g. via regulating the activity of a transcriptional regulator) or perhaps both remains to be determined. Furthermore, since HDACs also target many non-histone proteins, we cannot rule out that non-chromatin effects of HDAC1 on targets important for $CD4^+$ T cell migration contribute to the observed alterations. Further studies are required to determine whether factors involved in T cell migration are posttranslationally modified by acetylation and whether the acetylation status is altered in the absence of HDAC1. Of note, our bioinformatic analysis also revealed an upregulation of genes associated with oxidative phosphorylation and a downregulation of genes associated with Th1, Th2 and ICOS:ICOSL Th signaling. It is conceivable that some of these dysregulated pathways contribute, in addition to the $CD4^+$ T cell migration defect, to the protection of $HDAC1^{cKO}$ mice against EAE.

In our study we also observed that HDAC1-deficient naïve $CD4^+$ T cells failed to induce disease in an adoptive $CD4^+$ T cell transfer colitis model. This correlated with severely reduced numbers of transferred HDAC1-deficient $CD4^+$ T cells in intestinal tissues in comparison to transferred WT $CD4^+$ T cells, while there was only a mild reduction in the frequencies $HDAC1^{cKO}$ $CD4^+$ T cells in the spleen and mLNs. Similar frequencies of $CD4^+$ T cells in the spleen and mLNs argue against a survival defect of transferred HDAC1-deficient $CD4^+$ T cells and rather suggest impaired intestinal recruitment of $CD4^+$ T cells in the absence of HDAC1. Lymphocyte homing to intestinal tissues is regulated via a complex network of several factors including integrins LFA-1 and $\alpha_4\beta_7$ [44]. LFA-1 expression on T cells is essential for colitis induction, since transfer of naïve CD11a-deficient [41,43] or CD18-deficient [42] $CD4^+$ T cells into $Rag1^{-/-}$ recipient mice does not induce colitis. Of note, the few $HDAC1^{cKO}$ $CD4^+$ T cells that localized to the small intestine expressed WT levels of CD11a/CD18 as opposed to $HDAC1^{cKO}$ $CD4^+$ T cells residing in spleens and mLNs, where CD11a and/or CD18 were expressed at lower levels compared to WT $CD4^+$ T cells. This shows a correlation of LFA-1 expression levels and the ability of

HDAC1-deficient CD4$^+$ T cells to migrate into intestinal tissues. Therefore, in addition to EAE [21] and collagen-induced arthritis [24], a T cell-specific deletion of HDAC1 also prevents the induction of colitis. Furthermore, the observed reduction in the expression of selectin ligands PSGL-1 (CD162), CD43 and CD44 in transferred HDAC1^{cKO} CD4$^+$ T cells might also contribute to disease protection in this model, although PSGL-1-deficient CD4$^+$ T cells are not impaired in inducing colitis [42]. The role of other selectin ligands in T cell transfer colitis however remains unclear and awaits further investigation [70].

Together, our data indicate that HDAC1 is essential for CD4$^+$ T cells to cross endothelial barriers and to enter tissues such as the CNS, synovial joints or the gut lamina propria and epithelium. Thus, our data reveal a novel function for HDAC1 in regulating CD4$^+$ T cell migration in autoinflammatory diseases.

Authorship contribution statement

Patricia Hamminger: Conceptualization, Methodology, Formal analysis, Investigation, Writing – original draft, Visualization, Funding acquisition. Luca Marchetti: Methodology, Formal analysis, Investigation. Teresa Preglej: Methodology, Investigation, Writing – review & editing. Rene Platzer: Methodology, Software, Formal analysis, Investigation, Visualization, Writing – review & editing. Ci Zhu: Methodology, Investigation, Formal analysis, Visualization. Anton Kamnev: Methodology, Software, Formal analysis, Investigation, Visualization, Writing – review & editing. Ramona Rica: Investigation, Writing – review & editing. Valentina Stolz: Investigation. Lisa Sandner: Investigation, Writing – review & editing. Marlis Alteneder: Investigation. Elisa Kaba: Methodology. Darina Waltenberger: Investigation. Johannes B. Huppa: Methodology, Resources, Writing – review & editing. Michael Trauner: Resources, Writing – review & editing. Christoph Bock: Resources, Data curation, Writing – review & editing. Ruth Lyck: Methodology, Resources. Jan Bauer: Methodology, Formal analysis, Investigation, Visualization, Writing – Review and Editing. Loïc Dupré: Methodology, Resources, Writing – review & editing. Christian Seiser: Methodology, Resources. Nicole Boucheron: Methodology, Writing – review & editing. Britta Engelhardt: Conceptualization, Methodology, Resources, Writing – review & editing, Supervision. Wilfried Ellmeier: Conceptualization, Data curation, Funding acquisition, Project administration, Supervision, Validation, Writing – original draft.

Declaration of competing interest

None.

Acknowledgements

The authors thank Michael Schuster for RNA-seq data processing and initial analysis, and the Biomedical Sequencing Facility at CeMM for assistance with next-generation sequencing.

Appendix A. Supplementary data

Supplementary data to this article can be found online at https://doi.org/10.1016/j.jaut.2021.102610.

Funding

W.E., C·B., N.B. and C.S. were supported by the Austrian Science Fund (FWF) Special Research Program F70. W.E. was supported by FWF projects P19930, P23641, P26193, P29790; and by the FWF and Medical University of Vienna doctoral programs (DK W1212) “Inflammation and Immunity” and (DOC 32 doc.fund) “TissueHome”. R.P. was supported by a predoctoral fellowship of the Boehringer Ingelheim Fonds. J.B.H. received funding from the Vienna Science and Technology Fund (WWTF-LS14-031). P.H. was supported by a DOC fellowship of the Austrian Academy of Sciences. M.T. was supported by the FWF and Medical University of Vienna doctoral programs (DK W1212) “Inflammation and Immunity”. L.D. was supported by the Vienna Science and Technology Fund (WWTF-LS16-060). B.E. and L.M. were supported by the European Union’s Horizon 2020 research and innovation programme under the Marie Skłodowska-Curie Grant Agreement No 675619- BtRAIN and B.E. was supported by the Swiss National Science Foundation grant N° SNSF 31003A_170131. N.B. was supported by the FWF project P30885.

References

[1] J.M. Fletcher, S.J. Lalor, C.M. Sweeney, N. Tubridy, K.H. Mills, T cells in multiple sclerosis and experimental autoimmune encephalomyelitis, Clin. Exp. Immunol. 162 (2010) 1–11.
[2] T. Korn, A. Kallies, T cell responses in the central nervous system, Nat. Rev. Immunol. 17 (2017) 179–194.
[3] H. Lassmann, M. Bradl, Multiple sclerosis: experimental models and reality, Acta Neuropathol. 133 (2017) 223–244.
[4] B. Engelhardt, P. Vajkoczy, R.O. Weller, The movers and shapers in immune privilege of the CNS, Nat. Immunol. 18 (2017) 123–131.
[5] S.A. Sonar, G. Lal, Blood-brain barrier and its function during inflammation and autoimmunity, J. Leukoc. Biol. 103 (2018) 839–853.
[6] R.P. McEver, C. Zhu, Rolling cell adhesion, Annu. Rev. Cell Dev. Biol. 26 (2010) 363–396.
[7] A. Zarbock, K. Ley, R.P. McEver, A. Hidalgo, Leukocyte ligands for endothelial selectins: specialized glycoconjugates that mediate rolling and signaling under flow, Blood 118 (2011) 6743–6751.
[8] T.A. Yednock, C. Cannon, L.C. Fritz, F. Sanchez-Madrid, L. Steinman, N. Karin, Prevention of experimental autoimmune encephalomyelitis by antibodies against alpha 4 beta 1 integrin, Nature 356 (1992) 63–66.
[9] J.L. Baron, J.A. Madri, N.H. Ruddle, G. Hashim, C.A. Janeway Jr., Surface expression of alpha 4 integrin by CD4 T cells is required for their entry into brain parenchyma, J. Exp. Med. 177 (1993) 57–68.
[10] B.J. Steffen, E.C. Butcher, B. Engelhardt, Evidence for involvement of ICAM-1 and VCAM-1 in lymphocyte interaction with endothelium in experimental autoimmune encephalomyelitis in the central nervous system in the SJL/J mouse, Am. J. Pathol. 145 (1994) 189–201.
[11] J. Greenwood, Y. Wang, V.L. Calder, Lymphocyte adhesion and transendothelial migration in the central nervous system: the role of LFA-1, ICAM-1, VLA-4 and VCAM-1. off, Immunology 86 (1995) 408–415.
[12] E.J. Gordon, K.J. Myers, J.P. Dougherty, H. Rosen, Y. Ron, Both anti-CD11a (LFA-1) and anti-CD11b (MAC-1) therapy delay the onset and diminish the severity of experimental autoimmune encephalomyelitis, J. Neuroimmunol. 62 (1995) 153–160.
[13] M. Laschinger, B. Engelhardt, Interaction of alpha4-integrin with VCAM-1 is involved in adhesion of encephalitogenic T cell blasts to brain endothelium but not in their transendothelial migration in vitro, J. Neuroimmunol. 102 (2000) 32–43.
[14] S. Man, B. Tucky, N. Bagheri, X. Li, R. Kochar, R.M. Ransohoff, alpha4 Integrin/FN-CS1 mediated leukocyte adhesion to brain microvascular endothelial cells under flow conditions, J. Neuroimmunol. 210 (2009) 92–99.
[15] K.J. Dugger, K.R. Zinn, C. Weaver, D.C. Bullard, S.R. Barnum, Effector and suppressor roles for LFA-1 during the development of experimental autoimmune encephalomyelitis, J. Neuroimmunol. 206 (2009) 22–27.
[16] O. Steiner, C. Coisne, R. Cecchelli, R. Boscacci, U. Deutsch, B. Engelhardt, et al., Differential roles for endothelial ICAM-1, ICAM-2, and VCAM-1 in shear-resistant T cell arrest, polarization, and directed crawling on blood-brain barrier endothelium, J. Immunol. 185 (2010) 4846–4855.
[17] D.H. Miller, O.A. Khan, W.A. Sheremata, L.D. Blumhardt, G.P. Rice, M.A. Libonati, et al., A controlled trial of natalizumab for relapsing multiple sclerosis, N. Engl. J. Med. 348 (2003) 15–23.
[18] C.H. Polman, P.W. O'Connor, E. Havrdova, M. Hutchinson, L. Kappos, D.H. Miller, et al., A randomized, placebo-controlled trial of natalizumab for relapsing multiple sclerosis, N. Engl. J. Med. 354 (2006) 899–910.
[19] W. Ellmeier, C. Seiser, Histone deacetylase function in CD4(+) T cells, Nat. Rev. Immunol. 18 (2018) 617–634.
[20] T. Narita, B.T. Weinert, C. Choudhary, Functions and mechanisms of non-histone protein acetylation, Nat. Rev. Mol. Cell Biol. 20 (2019) 156–174.
[21] L. Göschl, T. Preglej, P. Hamminger, M. Bonelli, L. Andersen, N. Boucheron, et al., A T cell-specific deletion of HDAC1 protects against experimental autoimmune encephalomyelitis, J. Autoimmun. 86 (2018) 51–61.
[22] R. Grausenburger, I. Bilic, N. Boucheron, G. Zupkovitz, L. El-Housseiny, R. Tschismarov, et al., Conditional deletion of histone deacetylase 1 in T cells leads to enhanced airway inflammation and increased Th2 cytokine production, J. Immunol. 185 (2010) 3489–3497.
[23] T. Preglej, P. Hamminger, M. Luu, T. Bulat, L. Andersen, L. Goschl, et al., Histone deacetylases 1 and 2 restrain CD4+ cytotoxic T lymphocyte differentiation, JCI Insight 5 (2020).
[24] L. Göschl, T. Preglej, N. Boucheron, V. Saferding, L. Muller, A. Platzer, et al., Histone deacetylase 1 (HDAC1): a key player of T cell-mediated arthritis, J. Autoimmun. 108 (2020) 102379.

[25] E. Bettelli, M. Pagany, H.L. Weiner, C. Linington, R.A. Sobel, V.K. Kuchroo, Myelin oligodendrocyte glycoprotein-specific T cell receptor transgenic mice develop spontaneous autoimmune optic neuritis, J. Exp. Med. 197 (2003) 1073–1081.
[26] C. Coisne, L. Dehouck, C. Faveeuw, Y. Delplace, F. Miller, C. Landry, et al., Mouse syngenic in vitro blood-brain barrier model: a new tool to examine inflammatory events in cerebral endothelium, Lab. Invest. 85 (2005) 734–746.
[27] C. Coisne, R. Lyck, B. Engelhardt, Live cell imaging techniques to study T cell trafficking across the blood-brain barrier in vitro and in vivo, Fluids Barriers CNS 10 (2013) 7.
[28] N.A. Morin, P.W. Oakes, Y.M. Hyun, D. Lee, Y.E. Chin, M.R. King, et al., Nonmuscle myosin heavy chain IIA mediates integrin LFA-1 de-adhesion during T lymphocyte migration, J. Exp. Med. 205 (2008) 195–205.
[29] J. Schindelin, I. Arganda-Carreras, E. Frise, V. Kaynig, M. Longair, T. Pietzsch, et al., Fiji: an open-source platform for biological-image analysis, Nat. Methods 9 (2012) 676–682.
[30] Y. Gao, M.L. Kilfoil, Accurate detection and complete tracking of large populations of features in three dimensions, Optic Express 17 (2009) 4685–4704.
[31] S. Picelli, O.R. Faridani, A.K. Bjorklund, G. Winberg, S. Sagasser, R. Sandberg, Full-length RNA-seq from single cells using Smart-seq2, Nat. Protoc. 9 (2014) 171–181.
[32] D. Kim, G. Pertea, C. Trapnell, H. Pimentel, R. Kelley, S.L. Salzberg, TopHat2: accurate alignment of transcriptomes in the presence of insertions, deletions and gene fusions, Genome Biol. 14 (2013) R36.
[33] C. Trapnell, A. Roberts, L. Goff, G. Pertea, D. Kim, D.R. Kelley, et al., Differential gene and transcript expression analysis of RNA-seq experiments with TopHat and Cufflinks, Nat. Protoc. 7 (2012) 562–578.
[34] D. Hainberger, V. Stolz, C. Zhu, M. Schuster, L. Muller, P. Hamminger, et al., NCOR1 orchestrates transcriptional landscapes and effector functions of CD4(+) T cells, Front. Immunol. 11 (2020) 579.
[36] L. Dupre, R. Houmadi, C. Tang, J. Rey-Barroso, T lymphocyte migration: an action movie starring the actin and associated actors, Front. Immunol. 6 (2015) 586.
[37] V. Rothhammer, S. Heink, F. Petermann, R. Srivastava, M.C. Claussen, B. Hemmer, et al., Th17 lymphocytes traffic to the central nervous system independently of alpha4 integrin expression during EAE, J. Exp. Med. 208 (2011) 2465–2476.
[38] M. Abadier, N. Haghayegh Jahromi, L. Cardoso Alves, R. Boscacci, D. Vestweber, S. Barnum, et al., Cell surface levels of endothelial ICAM-1 influence the transcellular or paracellular T-cell diapedesis across the blood-brain barrier, Eur. J. Immunol. 45 (2015) 1043–1058.
[39] N. Haghayegh Jahromi, L. Marchetti, F. Moalli, D. Duc, C. Basso, H. Tardent, et al., Intercellular adhesion molecule-1 (ICAM-1) and ICAM-2 differentially contribute to peripheral activation and CNS entry of autoaggressive Th1 and Th17 cells in experimental autoimmune encephalomyelitis, Front. Immunol. 10 (2019) 3056.
[40] I. Wimmer, S. Tietz, H. Nishihara, U. Deutsch, F. Sallusto, F. Gosselet, et al., PECAM-1 stabilizes blood-brain barrier integrity and favors paracellular T-cell diapedesis across the blood-brain barrier during neuroinflammation, Front. Immunol. 10 (2019) 711.
[41] K.P. Pavlick, D.V. Ostanin, K.L. Furr, F.S. Laroux, C.M. Brown, L. Gray, et al., Role of T-cell-associated lymphocyte function-associated antigen-1 in the pathogenesis of experimental colitis, Int. Immunol. 18 (2006) 389–398.
[42] D.V. Ostanin, K.L. Furr, K.P. Pavlick, L. Gray, C.G. Kevil, D. Shukla, et al., T cell-associated CD18 but not CD62L, ICAM-1, or PSGL-1 is required for the induction of chronic colitis, Am. J. Physiol. Gastrointest. Liver Physiol. 292 (2007) G1706–G1714.
[43] I. Koboziev, F. Karlsson, D.V. Ostanin, L. Gray, M. Davidson, S. Zhang, et al., Role of LFA-1 in the activation and trafficking of T cells: implications in the induction of chronic colitis, Inflamm. Bowel Dis. 18 (2012) 2360–2370.
[44] A. Habtezion, L.P. Nguyen, H. Hadeiba, E.C. Butcher, Leukocyte trafficking to the small intestine and colon, Gastroenterology 150 (2016) 340–354.
[45] K. Ley, G.S. Kansas, Selectins in T-cell recruitment to non-lymphoid tissues and sites of inflammation, Nat. Rev. Immunol. 4 (2004) 325–335.
[46] K. Ley, C. Laudanna, M.I. Cybulsky, S. Nourshargh, Getting to the site of inflammation: the leukocyte adhesion cascade updated, Nat. Rev. Immunol. 7 (2007) 678–689.
[47] L. Marchetti, B. Engelhardt, Immune cell trafficking across the blood-brain barrier in the absence and presence of neuroinflammation, Vasc Biol 2 (2020) H1–H18.
[48] B.L. Walling, M. Kim, LFA-1 in T Cell migration and differentiation, Front. Immunol. 9 (2018) 952.
[49] N.H. Roy, S.H.J. Kim, A. Buffone Jr., D. Blumenthal, B. Huang, S. Agarwal, et al., LFA-1 signals to promote actin polymerization and upstream migration in T cells, J. Cell Sci. 133 (2020).
[50] S. Dusi, S. Angiari, E.C. Pietronigro, N. Lopez, G. Angelini, E. Zenaro, et al., LFA-1 controls Th1 and Th17 motility behavior in the inflamed central nervous system, Front. Immunol. 10 (2019) 2436.
[51] Z. Shulman, V. Shinder, E. Klein, V. Grabovsky, O. Yeger, E. Geron, et al., Lymphocyte crawling and transendothelial migration require chemokine triggering of high-affinity LFA-1 integrin, Immunity 30 (2009) 384–396.
[52] J. Greenwood, S.J. Heasman, J.I. Alvarez, A. Prat, R. Lyck, B. Engelhardt, Review: leucocyte-endothelial cell crosstalk at the blood-brain barrier: a prerequisite for successful immune cell entry to the brain, Neuropathol. Appl. Neurobiol. 37 (2011) 24–39.
[53] R. Lyck, B. Engelhardt, Going against the tide–how encephalitogenic T cells breach the blood-brain barrier, J. Vasc. Res. 49 (2012) 497–509.
[54] C.V. Carman, P.T. Sage, T.E. Sciuto, M.A. de la Fuente, R.S. Geha, H.D. Ochs, et al., Transcellular diapedesis is initiated by invasive podosomes, Immunity 26 (2007) 784–797.
[55] C.V. Carman, Mechanisms for transcellular diapedesis: probing and pathfinding by 'invadosome-like protrusions', J. Cell Sci. 122 (2009) 3025–3035.
[56] R. Martinelli, A.S. Zeiger, M. Whitfield, T.E. Sciuto, A. Dvorak, K.J. Van Vliet, et al., Probing the biomechanical contribution of the endothelium to lymphocyte migration: diapedesis by the path of least resistance, J. Cell Sci. 127 (2014) 3720–3734.
[57] M. Sperandio, C.A. Gleissner, K. Ley, Glycosylation in immune cell trafficking, Immunol. Rev. 230 (2009) 97–113.
[58] M.L. Ford, T.M. Onami, A.I. Sperling, R. Ahmed, B.D. Evavold, CD43 modulates severity and onset of experimental autoimmune encephalomyelitis, J. Immunol. 171 (2003) 6527–6533.
[59] F. Velazquez, A. Grodecki-Pena, A. Knapp, A.M. Salvador, T. Nevers, K. Croce, et al., CD43 functions as an E-selectin ligand for Th17 cells in vitro and is required for rolling on the vascular endothelium and Th17 cell recruitment during inflammation in vivo, J. Immunol. 196 (2016) 1305–1316.
[60] S.M. Kerfoot, P. Kubes, Overlapping roles of P-selectin and alpha 4 integrin to recruit leukocytes to the central nervous system in experimental autoimmune encephalomyelitis, J. Immunol. 169 (2002) 1000–1006.
[61] S.M. Kerfoot, M.U. Norman, B.M. Lapointe, C.S. Bonder, L. Zbytnuik, P. Kubes, Reevaluation of P-selectin and alpha 4 integrin as targets for the treatment of experimental autoimmune encephalomyelitis, J. Immunol. 176 (2006) 6225–6234.
[62] R.L. Camp, A. Scheynius, C. Johansson, E. Pure, CD44 is necessary for optimal contact allergic responses but is not required for normal leukocyte extravasation, J. Exp. Med. 178 (1993) 497–507.
[63] J. Lesley, R. Hyman, P.W. Kincade, CD44 and its interaction with extracellular matrix, Adv. Immunol. 54 (1993) 271–335.
[64] H.C. DeGrendele, P. Estess, L.J. Picker, M.H. Siegelman, CD44 and its ligand hyaluronate mediate rolling under physiologic flow: a novel lymphocyte-endothelial cell primary adhesion pathway, J. Exp. Med. 183 (1996) 1119–1130.
[65] H.C. DeGrendele, P. Estess, M.H. Siegelman, Requirement for CD44 in activated T cell extravasation into an inflammatory site, Science 278 (1997) 672–675.
[66] M. Nacher, A.B. Blazquez, B. Shao, A. Matesanz, C. Prophete, M.C. Berin, et al., Physiological contribution of CD44 as a ligand for E-Selectin during inflammatory T-cell recruitment, Am. J. Pathol. 178 (2011) 2437–2446.
[67] S. Brocke, C. Piercy, L. Steinman, I.L. Weissman, T. Veromaa, Antibodies to CD44 and integrin alpha4, but not L-selectin, prevent central nervous system inflammation and experimental encephalomyelitis by blocking secondary leukocyte recruitment, Proceedings of the National Academy of Sciences of the United States of America 96 (1999) 6896–6901.
[68] F.R. Brennan, J.K. O'Neill, S.J. Allen, C. Butter, G. Nuki, D. Baker, CD44 is involved in selective leucocyte extravasation during inflammatory central nervous system disease, Immunology 98 (1999) 427–435.
[69] P. Johnson, B. Ruffell, CD44 and its role in inflammation and inflammatory diseases, Inflamm. Allergy - Drug Targets 8 (2009) 208–220.
[70] J. Rivera-Nieves, G. Gorfu, K. Ley, Leukocyte adhesion molecules in animal models of inflammatory bowel disease, Inflamm. Bowel Dis. 14 (2008) 1715–1735.
[71] Moolenbeek, Ruitenberg, The 'Swiss roll': a simple technique for histological studies of the rodent intestine, Laboratory Animals 15 (1981) 57–59, https://doi.org/10.1258/002367781780958577. In press.